Mon. Not. R. astr. Soc. (1974) **166,** 19–55.

RADIATIVE TRANSFER IN SPHERICALLY SYMMETRIC SYSTEMS—III

Fundamentals of line Formation

P. B. Kunasz and D. G. Hummer

(Received 1973 August 3)

SUMMARY

A generalization of the variable Eddington factor method is presented that makes possible the solution of line formation problems in extended spherical atmospheres whose constitutive properties depend on radius in an arbitrary way. Extensive numerical results for Doppler broadening in models with power law opacities ($n = 0, 2, 3$) are presented and interpreted. Very substantial deviations are found from the solutions of analogous plane-parallel models. The single-flight escape probability is derived for a general opacity law and is shown to exceed that for an analogous plane-parallel slab by no more than a factor of approximately two for Doppler broadening, or three-halves for Lorentz broadening. However, it is shown that each time a photon is scattered, it has a probability greater than one-half of ending its flight at a radius larger than that at which it was emitted. This effect is peculiar to spherical geometries and may be important in aiding the escape of photons from optically thick systems. Finally the effects of dilution are considered and some properties of the infinite radius, finite optical depth models are inferred. An appendix contains the solution of the line transfer problem for a homogeneous sphere by the kernel-approximation method.

1. INTRODUCTION

The problem of spectral line formation in extended atmospheres has increased in importance as the observations of strong lines in giant and supergiant stars, novae and Wolf–Rayet stars have improved and become more readily available. This problem is also of particular theoretical interest because of the circumstance that the ratio of photon mean free path to radius of curvature of each layer in the atmosphere, which must be small for the plane-parallel approximation to hold, can become large in the line wings even if it is quite small near the centre of the line.

In order to elucidate the effects on line formation of deviations from the familiar plane-parallel geometry, we limit our attention here to *static* spherical atmospheres in which the opacity is a prescribed function of radius and frequency. Throughout this paper, our results are compared with the corresponding ones for the analogous plane-parallel atmosphere. This discussion is based largely on results obtained from a powerful and general numerical technique, a generalization of the variable Eddington-factor method discussed in the two earlier papers of this series, Hummer & Rybicki (1971a) and Cassinelli & Hummer (1971), which we shall refer to as Papers I and II, respectively. This method is developed in Section 2 for a more general model than is considered in the remainder of this paper, and has been used to obtain results of more relevance to the interpretation of stellar observations than are those to be discussed here. (This work provides the basis for the construction of spherical, non-LTE model stellar atmospheres.) Because of the intimate

relation between extension and the radial flow of the gases in the atmosphere, a procedure to include a macroscopic velocity field has been developed, and will be published later in this series of papers.

In Section 3 a number of theoretical concepts are developed that are useful in understanding the basic features of line formation in spherical systems. In Section 4 the numerical results for power law opacities with exponents of $n = 0, 2, 3$ are discussed. An appendix is devoted to the solution of the integral equation for the source function in a homogeneous sphere.

The problems of line formation in media with spherical symmetry have received very little attention and, then, only for models in which the opacity is independent of radius. Cuperman, Englemann & Oxenius (1963, 1964) have obtained some numerical results for small and moderate optical thicknesses. The problem of line formation in an infinite homogeneous medium containing a point source has been discussed by Nagirner & Ivanov (1966) and Ivanov & Nagirner (1966). The mean number of scatterings in a homogeneous spherical atmosphere with a uniform distribution of sources is treated exactly by Ivanov (1969, 1970). These and other aspects of line formation in homogeneous spherical atmospheres are discussed and summarized by Ivanov (1973). Mathis (1968) used Λ-iteration to obtain numerical results for a homogeneous sphere and, very recently, Grant & Peraiah (1972) have examined line formation in a homogeneous shell in which the ratio of outer to inner radius does not exceed two.

However, it should be noted that a constant opacity law constitutes a special case in which the effects of the spherical geometry do not develop fully. To see this, we consider the family of opacity laws $k(r) = kr^{-n}$. The ratio of photon mean free path to radius of curvature is $\lambda/r = r^{n-1}/k$. We recall that this ratio is zero for plane-parallel situations. For $n = 0$, this ratio is proportional to r^{-1} and therefore becomes small as r increases, while for $n > 1$, it increases with r and can become very large. Thus deviations from plane-parallel geometries are minimized for constant opacities and develop fully only when $n > 1$.

We may remark in passing that the anomalous case $n = 1$, in which $\lambda/r = k^{-1}$, separates these two classes of behaviour. In this case the effect of spherical geometry can be made arbitrarily large or small by the value of k that is chosen, and a variety of exact results has been found by Aamodt (1962), Schmid-Burgk (1973) and Rybicki (1970, private communication). This case seems quite unphysical. For example, when the outer radius of the system is infinite, the angular distribution of the radiation is independent of radius and is determined only by the parameter k. When k is large, very substantial deviations from isotropy occur (the distribution can become singular) so that, as Schmid-Burgk (1973) has stressed, the Eddington factor never becomes $1/3$. However, it is difficult to imagine a physical situation in which the ratio of mean free path to radius is constant; moreover, as this ratio becomes extremely small at large depths for any object, Schmid-Burgk's concern that the Eddington factor $f = K/J$ need not approach $1/3$ when the monochromatic optical depth is large seems largely academic.

2. THE VARIABLE EDDINGTON FACTOR PROCEDURE FOR LINES

The transfer equation for the radiation field in a spectral line can be written as

$$\mu \frac{\partial}{\partial r} I(x, \mu, r) + \frac{1-\mu^2}{r} \frac{\partial I}{\partial \mu}(x, \mu, r) = -k(x, r)[I(x, \mu, r) - S(r)], \qquad (2.1)$$

where we ignore continuous absorption and emission. Here x is the frequency displacement from line centre, measured in terms of a standard frequency interval such as the Doppler width at some fixed temperatures, μ is the cosine of the angle between the direction of propagation and the outward directed radius vector and r is the distance from the centre of symmetry. As we are throughout this paper assuming complete frequency redistribution, the line source function for the standard two-level atomic model can be written as

$$S(r) = (1-\epsilon)\int_{-\infty}^{\infty} dx\phi(x, r)\, J(x, r)+\epsilon B, \tag{2.2}$$

where $\phi(x, r)$ is the frequency dependence of the opacity normalized to unity on the x-scale at every depth, $\epsilon(r)$ is the probability per scattering that a photon is lost from the line and $B(r)$ is the Planck function at the line centre for the local electron temperature. In this procedure $k(x, r)$, $\epsilon(r)$, $B(r)$ and $\phi(x, r)$ are arbitrary functions of depth and frequency. It will be convenient later to introduce the notation

$$k(r) = \int_{-\infty}^{\infty} dx\, k(x, r),$$

which expresses the normalization of $\phi(x, r)$, i.e. $k(x, r) = k(r)\,\phi(x, r)$.

We assume a geometrical configuration consisting of a shell of outer radius R surrounding a core of radius R_c, and consider two cases: (1) the core is hollow; (2) the core is perfectly absorbing and emits a specified radiation field in the vicinity of the line which can, of course, have zero intensity.

The zeroth and first moments of (2.1) with respect to μ are

$$r^{-2}\frac{\partial}{\partial r}[r^2H(x, r)] = -k(x, r)[J(x, r)-S(r)] \tag{2.3}$$

and

$$\frac{\partial}{\partial r}K(x, r)-\frac{1}{r}[J(x, r)-3K(x, r)] = -k(x, r)\,H(x, r), \tag{2.4}$$

where

$$J(x, r) = \tfrac{1}{2}\int_{-1}^{1} d\mu\, I(x, \mu, r), \tag{2.5a}$$

$$H(x, r) = \tfrac{1}{2}\int_{-1}^{1} d\mu\, \mu I(x, \mu, r), \tag{2.5b}$$

$$K(x, r) = \tfrac{1}{2}\int_{-1}^{1} d\mu\, \mu^2 I(x, \mu, r). \tag{2.5c}$$

Let us define the so-called Eddington factors

$$f(x, r) = K(x, r)/J(x, r) \tag{2.6a}$$

and

$$g(x, r) = H(x, r)/J(x, r). \tag{2.6b}$$

We can now rewrite (2.4) as (omitting r and x for brevity)

$$\frac{\partial}{\partial r}(fJ)-\frac{1}{r}(1-3f)\,J = -kH. \tag{2.7}$$

Following Auer (1971), we introduce the integrating factor q, defined by

$$\frac{1}{q}\frac{\partial q}{\partial r} = (3f-1)/rf, \tag{2.8}$$

in terms of which (2.7) takes the form

$$\frac{1}{q}\frac{\partial}{\partial r}(fqJ) = -kH. \tag{2.9}$$

To make things definite, we shall use the solution of (2.8)

$$q(x, r) = \exp\left\{\int_{R_c}^{r} dr(3f-1)/rf\right\}. \tag{2.10}$$

By differentiating (2.9) with respect to r, we can eliminate H from (2.3) to obtain the *combined moment equation*

$$r^{-2}\frac{\partial}{\partial r}\left[\frac{r^2}{kq}\frac{\partial}{\partial r}(fqJ)\right] = k(J-S). \tag{2.11}$$

The specification of the two-point boundary value problem for J is completed by eliminating H between (2.6b) and (2.9) and imposing the resulting expression

$$\frac{1}{q}\frac{\partial}{\partial r}(fqJ) = -kgJ, \tag{2.12}$$

at $r = R_c$ and $r = R$. We note that (2.11) and (2.12) hold for each frequency of interest; the equations for all frequencies are coupled through S, as is clear from (2.2).

The strategy is as follows. If f is specified for all r and x, and g, for all x at $r = R_c$ and R, then q is known as well, and J can be found from (2.11) and (2.12) if S can be expressed approximately as a linear combination of J at discrete frequencies. When J is known, $S(r)$ can be calculated and the formal solution of (2.1) evaluated to give I and hence J, H and K. By calculating the Eddington factors from (2.5), the process can be repeated to convergence. As suggested by the results of Papers I and II, convergence is very rapid. The very different length scales associated with the different frequencies do not appear to have caused any instability.

Since the practicability of this procedure depends on the power of the numerical methods and on the efficiency with which they are employed, the solution of the moment equation (2.11) and the calculation of the formal solution are described in some detail in the next two subsections.

2.1 *Solution of the moment equation*

The natural variable appears to be

$$y(x, r) = f(x, r)\, q(x, r)\, J(x, r). \tag{2.13}$$

If we now introduce a set of discrete frequency variables x^i, $i = 1, 2, \ldots, N$, and a quadrature formula of the form

$$\int_{-\infty}^{\infty} dx\, \phi(x, r)\, J(x, r) = \sum_{i=1}^{N} W^i(r)\, J(x^i, r), \tag{2.14}$$

we can write (2.11) and (2.2) as

$$r^{-2}\frac{\partial}{\partial r}\left[\frac{r^2}{k^i(r)\,q^i(r)}\frac{\partial}{\partial r}y^i(r)\right] = k^i(r)\left[\frac{y^i(r)}{f^i(r)\,q^i(r)} - S(r)\right],$$
$$i = 1, 2, \ldots, N, \tag{2.15}$$

and

$$S(r) = (1-\epsilon)\sum_{i=1}^{N} W^i(r)\,y^i(r)/f^i(r)\,q^i(r) + \epsilon B, \tag{2.16}$$

where the superscript i on a quantity denotes its association with the frequency x^i.

This system could be solved by the use of difference equations, as outlined in Paper II. Instead, we will use a more accurate procedure related to the theory of cubic spline interpolation (see, for example, Ahlberg, Nilson & Walsh 1967, Chapter 1). We introduce an optical-depth-like independent variable t^i by the relation

$$\frac{d}{dt^i} = \frac{r^2}{k^i q^i}\frac{d}{dr}, \tag{2.17}$$

in terms of which (2.15) takes the form

$$\frac{d^2}{(dt^i)^2}y^i = \frac{r^4}{q^i}\left[\frac{y^i}{f^i q^i} - S(r)\right], \quad i = 1, 2, \ldots, N. \tag{2.18}$$

The boundary conditions (2.12) are now expressed as

$$\frac{d}{dt^i}y^i = -\frac{r^2 g^i}{q^i f^i}y^i, \quad r = R_c, R. \tag{2.19}$$

Although the independent variables $\{t^i\}$ will all be related to r in different ways, the arguments of y^i in the source function all refer to the same value of r.

Let us now assume that each function $y^i(t^i)$ is piecewise cubic and that it and its first two derivatives are continuous at each of the radial grid points. We shall use the subscript j with any number of primes to label the radius points; superscripts i and i' continue to label frequency points and will be suppressed when possible. We emphasize that all $t_j{}^i$ with the same value of j refer to a common radial point, r_j. Thus, we define, for $j = 1, 2, \ldots, Q$,

$$y_j = y^i(t_j{}^i), \tag{2.20}$$

$$M_j = \frac{d^2}{(dt^i)^2}y^i\Big|_{t^i = t_j{}^i}, \tag{2.21}$$

and

$$h_j = t_j{}^i - t_{j-1}{}^i. \tag{2.22}$$

It is easily verified that if $y(t)$ is a piecewise cubic function in the interval $t_{j-1} \le t \le t_j$ it can be written as

$$y(t) = [M_{j-1}(t_j - t)^3 + M_j(t - t_{j-1})^3 + (6y_{j-1} - M_{j-1}h_j^2)(t_j - t) + (6y_j - M_j h_j^2)(t - t_{j-1})]/6h_j. \tag{2.23}$$

The first two derivatives are

$$y'(t) = [-3M_{j-1}(t_j - t)^2 + 3M_j(t - t_{j-1})^2 - (6y_{j-1} - M_{j-1}h_j^2) + (6y_j - M_j h_j^2)]/6h_j \tag{2.24}$$

and

$$y''(t) = [M_{j-1}(t_j - t) + M_j(t - t_{j-1})]/h_j. \tag{2.25}$$

It is clear from the expressions for y and y'' that they are continuous at the nodes t_j. Requiring y' to be continuous at the nodes leads to the expression

$$y_{j-1}h_{j+1}-y_j(h_j+h_{j+1})+y_{j+1}h_j = \tfrac{1}{6}h_jh_{j+1}[h_jM_{j-1}+2(h_j+h_{j+1})M_j+h_{j+1}M_{j+1}]. \quad (2.26)$$

In spline interpolation theory, this relation, when augmented by boundary conditions, provides a tri-diagonal system for the unknowns M_j in terms of the known quantities y_j. Here, however, we see from (2.18) that

$$M_j = \frac{r_j^4}{q_j}\left(\frac{y_j}{f_jq_j}-S_j\right), \quad (2.27)$$

which, when substituted into (2.26), gives a tridiagonal system for the quantities y_j,

$$y_{j-1}\left[\frac{1}{h_j}-\frac{1}{6}\frac{h_jr_{j-1}^4}{f_{j-1}q_{j-1}^2}\right]-y_j\left(\frac{1}{h_j}+\frac{1}{h_{j+1}}\right)\left(1+\frac{h_jh_{j+1}r_j^4}{3f_jq_j^2}\right)+y_{j+1}\left[\frac{1}{h_{j+1}}-\frac{1}{6}\frac{h_{j+1}r_{j+1}^4}{f_{j+1}q_{j+1}^2}\right]$$
$$= -\frac{1}{6}\left[\frac{h_jr_{j-1}^4}{q_{j-1}}S_{j-1}+2\frac{(h_j+h_{j+1})}{q_j}r_j^4S_j+\frac{h_{j+1}r_{j+1}^2}{q_{j+1}}S_{j+1}\right], \quad j=1,2,\ldots,Q. \quad (2.28)$$

These equations must be augmented by those expressing the boundary conditions at $r = R_c$ and $r = R$.

We note in passing that $q^i(r)$ is computed from (2.8) by means of a cubic spline representation of $f^i(r)$; and similarly, $t^i(r)$ is evaluated from (2.17) using cubic representations of $f^i(r)$ and $q^i(r)$.

2.2 *Boundary conditions*

The effect of the boundaries is specified by the Eddington factors f^i and g^i in (2.19). At the outer boundary of the atmosphere these factors are determined iteratively; the condition that no radiation is incident enters explicitly in the formal solution, as will be discussed in Section 2.3. From (2.19), (2.24) and (2.27) we obtain, for the condition at the outer boundary,

$$y_Q\left[\frac{g_QR^2}{f_Qq_Q}+\frac{1}{h_Q}+\frac{1}{3}\frac{h_QR^4}{f_Qq_Q^2}\right]-y_{Q-1}\left[\frac{1}{h_Q}-\frac{1}{6}\frac{h_Qr_{Q-1}^4}{f_{Q-1}q_{Q-1}^2}\right]$$
$$= -\frac{1}{6}\frac{h_Qr_{Q-1}^4}{q_{Q-1}}S_{Q-1}-\frac{1}{3}\frac{h_QR^4}{q_{Q-1}}S_Q. \quad (2.29)$$

If the core is hollow, then for each frequency the flux at $r = R_c$ is zero, i.e. $g^i = 0$, so that our expression for the inner boundary condition is

$$y_1\left[\frac{1}{h_2}+\frac{1}{3}\frac{h_2R_c^4}{f_1q_1^2}\right]-y_2\left[\frac{1}{h_2}-\frac{1}{6}\frac{h_2r_2^4}{f_2q_2^4}\right] = \frac{1}{3}\frac{h_2R_c^4}{q_1}S_1+\frac{1}{6}h_2\frac{r_2^4}{q_2}S_2. \quad (2.30)$$

For an opaque, emitting core one can, in principle, use f and g as determined by the formal solution. We have found that the numerical accuracy can be substantially improved by treating the core radiation field in a more explicit way. At the inner boundary $r = R_c$ we define the 'half-range' moments for radiation of

frequency x^i,

$$J^{i\pm} = \tfrac{1}{2}\int_0^1 d\mu\, I^i(\pm\mu), \tag{2.31}$$

and

$$H^{i\pm} = \tfrac{1}{2}\int_0^1 d\mu\, \mu I^i(\pm\mu). \tag{2.32}$$

Obviously

$$J^i = J^{i+} + J^{i-} \tag{2.33a}$$

and

$$H^i = H^{i+} - H^{i-}. \tag{2.33b}$$

The quantities with 'plus' superscripts are known when the radiation field produced by the core is specified.

Let us now define an Eddington flux factor for radiation in the inward hemisphere ($\mu < 0$),

$$g^{i-} = H^{i-}/J^{i-}. \tag{2.34}$$

The monochromatic flux at $r = R_c$ can then be written as

$$H^i = H^{i+} - g^{i-}J^{i-} = H^{i+} - g^{i-}(J^i - J^{i+}). \tag{2.35}$$

We can therefore rewrite (2.19) as

$$\frac{d}{dt}y^i = -r^2\left[H^{i+} - g^{i-}\left(\frac{y^i}{f^i g^i} - J^{i+}\right)\right], \quad r = R_c. \tag{2.36}$$

The quantities H^{i+} and J^{i+} are known and g^{i-}, f^i and q^i are obtained iteratively from the formal solution. The discrete form of (2.36) is

$$y_1\left[\frac{1}{h_2} + \frac{1}{3}\frac{h_2 R_c^4}{f_1 q_1} - \frac{g^- R_c^2}{f_1 q_1}\right] - y_2\left[\frac{1}{h_2} - \frac{1}{6}\frac{h_2 r_2^4}{f_2 q_2}\right]$$
$$= \frac{1}{3}h_2\frac{R_c^4}{q_1}S_1 + \frac{1}{6}h_2\frac{r_2^4}{q_2}S_2 + R_c^2[H^+ - g^- J^+], \tag{2.37}$$

which provides the condition at the inner boundary for an opaque core that emits an arbitrary spectrum.

We now have specified completely a tridiagonal linear system for the quantities y_j. Since however, each y_j is really an N-dimensional vector with components y_j^i which are coupled together through the source function, the matrix of the system is block-tridiagonal with dimension Q, each block having dimensions $N \times N$. The system is solved by the usual technique first used for transfer problems by Feautrier (1964). The system matrix is reduced to block upper-triangular form, from which the y_j are found by back substitution. Because, in (2.28), the source function at all three points is involved, all of the submatrices are full, so that a large number of $N \times N$ matrices must be inverted.

2.3 *Formal solution*

The formal solution, that is, the evaluation of the intensity from a given source function, opacity and set of boundary conditions, was calculated in much the same way as was done in Papers I and II. The procedure was improved in several respects,

leading to significant increases in accuracy, speed and generality, and to a reduction in the amount of computer storage required. Hummer, Kunasz & Kunasz (1973) gives a detailed description of the method and the associated code; the latter, which is of general applicability for the evaluation of formal solutions in spherical geometry, can be obtained from the *Computer Physics Communications* Program Library. A brief outline of the method will suffice here.

The transfer equation is integrated along parallel rays parameterized by the perpendicular distance from the centre, i.e. by the impact parameter p (*cf.* Fig. 1 of Paper I). At the inner boundary $r = R_c$, either a hollow core or an opaque core emitting a specified radiation field can be assumed; at the outer boundary it is assumed that no radiation is incident from the outside. The equations were differenced by assuming that the radiation quantities are piece-wise cubic and were continuous, along with the first and second derivative at the points of the (r, p) grid. The moments J, H and K were evaluated through the use of spline-based quadrature formulae, and the calculation was organized in such a way that the contributions to each moment could be accumulated as the transfer equation was integrated along each ray. This procedure eliminated the need to store the intensity at all spatial grid points for a given frequency in order to calculate the moments at that frequency.

2.4 *Practical considerations*

We have coded the procedure just described, with obvious generalizations to account for continuum processes, for the CDC 6400. We have had about six months of experience with this code and find that, once insight has been acquired in selecting the radius and impact parameter grids, the procedure works very well for a variety of problems. An opacity law of the form

$$k(x, r) = k(r)\,\phi(x) \tag{2.38}$$

was used, and for the cases reported in this paper, pure Doppler broadening was assumed, i.e.

$$\phi(x) = \frac{1}{\sqrt{\pi}}\,e^{-x^2}. \tag{2.39}$$

The results of calculations in which $k(r) = Kr^{-n}$, $n = 0, 2, 3$ are discussed in Section 4.

Up to ten equally spaced frequency points were used for $x \geq 0$ in evaluating the scattering integral in (2.14) with trapezoidal weights renormalized to insure that the normalization condition

$$\int_{-\infty}^{\infty} dx\,\phi(x) = 1$$

is fulfilled exactly. For $R \lesssim 300\,R_c$ and $T \lesssim 10^3$, typically 60 radial points were used in integrating the moment equation and 100 radial points and 50 impact parameters were used in the formal solution. Normally three iterations were required, which, for a typical problem, took on the order of 100 s of central processor time. On the basis of comparisons with the results of independent calculations for plane-parallel and for homogeneous sphere problems, we believe that the maximum error in this method using the grid sizes indicated is on the order of 2 or 3 per cent.

3. THEORETICAL CONCEPTS

In this section we develop several theoretical concepts that are essential for understanding the fundamental aspects of line formation in spherical systems. The concepts are used in Section 4 in the interpretation of numerical data. The single-flight escape probability is familiar from plane-parallel theory, while the bias in scattering to larger radii and dilution are characteristic of spherical systems. The concepts of mean number of scatterings and mean escape probabilities and their relation to the single-flight escape probability are discussed briefly.

3.1 *Single-flight escape probability*

We use this term to describe the probability that a photon emitted at a specific point in the atmosphere will subsequently escape without further scattering. The utility of this concept in understanding the gross features of line transfer problems in plane-parallel media is discussed, for example, by Hummer & Rybicki (1971b). By a simple argument, due apparently to Zanstra (1949), it is easy to show that for a plane-parallel atmosphere the single-flight escape probability from optical depth τ in an atmosphere of optical thickness T is

$$P_{\rm pl}(\tau) = \tfrac{1}{2}[K_2(\tau)+K_2(T-\tau)], \tag{3.1}$$

where

$$K_2(\tau) = \int_{-\infty}^{\infty} dx\, \phi(x)\, E_2(\tau\phi(x)). \tag{3.2}$$

Here E_2 is the second exponential-integral function, x is a dimensionless frequency displacement from line centre and $\phi(x)$ is the frequency dependence of the absorption coefficient normalized to unity.

Let us consider the geometrical model discussed in Section 2 and for simplicity assume that the central core is hollow. We imagine an excited atom at radius r, which emits a photon of frequency x, $x+dx$ with probability $\phi(x)\,dx$. The probability that the direction of propagation lies within the element of solid angle $d\Omega$ is $d\Omega/4\pi = \frac{1}{2}\,d\mu$. In the (p, r) system, we find that the probability that a photon is emitted with its impact parameter between p and $p+dp$, propagating in *either* the positive or negative direction is $p\,dp/2r\sqrt{r^2-p^2}$. Note that the path of a photon emitted by an atom at radius r has an impact parameter p that cannot exceed r. Finally the probability that a photon of frequency x escapes in the positive direction is

$$\alpha^+(r, p, x) = \exp\left\{-\int_{\sqrt{r^2-p^2}}^{\sqrt{R^2-p^2}} k(x, r = \sqrt{z^2+p^2})\, dz\right\}; \tag{3.3}$$

that in the negative direction is

$$\alpha^-(r, p, x) = \exp\left\{-\int_{z_0(p)}^{\sqrt{r^2-p^2}} k(x, r = \sqrt{z^2+p^2})\, dz - \int_{z_0(p)}^{\sqrt{R^2-p^2}} k(x, r = \sqrt{z^2+p^2})\, dz\right\}, \tag{3.4}$$

where

$$z_0(p) = \begin{cases} 0, & p > R_c, \\ \sqrt{R_c^2-p^2}, & p \le R_c. \end{cases} \tag{3.5}$$

Consequently the single-flight escape probability for a photon emitted at radius r is

$$P(r) = \frac{1}{2}\int_0^r dp \frac{p}{r\sqrt{r^2-p^2}} \int_{-\infty}^{\infty} dx\, \phi(x)[\alpha^+(r, p, x)+\alpha^-(r, p, x)]. \quad (3.6)$$

Let us now write the opacity in the form

$$k(x, r) = K\phi(x)\not{f}(r), \quad (3.7)$$

where the separation between K and $\not{f}(r)$ is arbitrary but convenient. By making the substitution $t = \sqrt{p^2+z^2}$, we can write α^+ and α^- as

$$\alpha^-(r, p, x) = \exp\{-K\phi(x)\, Z^+(r, p)\} \quad (3.8)$$

and

$$\alpha^+(r, p, x) = \exp\{-2K\phi(x)\, Z^-(r, p)-K\phi(x)\, Z^+(r, p)\}. \quad (3.9)$$

Here

$$Z^+(r, p) = \int_r^R dt\, t\not{f}(t)/\sqrt{t^2-p^2} \quad (3.10)$$

and

$$Z^-(r, p) = \int_{r_0(p)}^r dt\, t\not{f}(t)/\sqrt{t^2-p^2}, \quad (3.11)$$

where

$$r_0(p) = \max(p, R_c). \quad (3.12)$$

When $p = 0$, these functions are simply related to the radial optical depth:

$$Z^+(r, 0) = \tau/K. \quad (3.13)$$

and

$$Z^-(r, 0) = (T-\tau)/K. \quad (3.14)$$

Additionally, $Z^+(r, p)$ is a monotonically increasing function of p.

We now introduce the *obliquity factors*, which are analogous to $1/\mu$ in the plane parallel case:

$$A^\pm(r, p) \equiv Z^\pm(r, p)/Z^\pm(r, 0). \quad (3.15)$$

These functions can be evaluated when $\not{f}(r)$ is specified. $A^+(r, p)$ increases monotonically with p and reaches a finite maximum when $p = r$. The corresponding function for the plane-parallel case is $(1-p^2/r^2)^{-1/2}$, which becomes infinite for $p = r$. Writing τ now as the argument and regarding $r = r(\tau)$, we have for the escape probability the expression

$$P(\tau) = \tfrac{1}{2}\int_0^r \mathrm{d}p \frac{p}{r\sqrt{r^2-p^2}} \int_{-\infty}^{\infty} dx\phi(x) \Big\{\exp[-\phi(x)\tau A^+(r, p)] \quad (3.16)$$

$$+ \exp[-\phi(x)(\tau A^+(r, p) + 2(T-\tau)\, A^-(r, p))]\Big\}.$$

In terms of the function

$$M_2(\tau) = \int_{-\infty}^{\infty} dx\phi(x)\, \mathrm{e}^{-\tau\phi(x)}, \quad (3.17)$$

we can write this result as

$$P(\tau) = \tfrac{1}{2}\int_0^r \frac{dp\, p}{r\sqrt{r^2-p^2}} \{M_2[\tau A^+(r, p)]+M_2[\tau A^+(r, p)+2(T-\tau)\, A^-(r, p)]\}. \quad (3.18)$$

It is readily shown that, by setting $A^+ = A^- = r/\sqrt{r^2-p^2}$, this expression reduces to that given above for the case of a plane-parallel atmosphere of thickness $2T$.

Before going on to discuss the asymptotic behaviour of this expression for Doppler and Lorentz profiles, it will be helpful to examine in detail the obliquity factors A^+ and A^- in some special cases.

3.1.1 *Obliquity factors.* By writing these quantities in the forms

$$A^+(r,p) = \int_r^R dt\, \phi(t)/\sqrt{1-(p/t)^2} \Big/ \int_r^R dt\, \phi(t) \tag{3.19}$$

and

$$A^-(r,p) = \int_{r_0(p)}^r dt\, \phi(t)/\sqrt{1-(p/t)^2} \Big/ \int_{R_c}^r dt\, \phi(t), \tag{3.20}$$

we see at once, since $\phi(r) > 0$, that

$$A^+(r,p) \leq 1/\sqrt{1-(p/r)^2}. \tag{3.21}$$

For $p > R_c$,

$$A^-(r,p) \geq 1/\sqrt{1-(p/r)^2} \int_p^r dt\, \phi(t) \Big/ \int_{R_c}^r dt\, \phi(t), \tag{3.22}$$

and for $p < R_c$

$$A^-(r,p) \leq 1/\sqrt{1-(p/R_c)^2}. \tag{3.23}$$

Thus we see that $A^+(r,p)$ is always smaller than for the plane-parallel case, while $A^-(r,p)$ can be larger, and for $p < R_c$ must be larger, than for the plane-parallel case. Thus photons escaping in the positive z-direction can escape more easily, while those escaping in the other direction may find it more difficult than in the corresponding plane-parallel case.

For opacity laws of the form $\phi(r) = r^{-n}$, $n \geq 0$, we can evaluate the functions $A^\pm$ in a form that is particularly easy to visualize. It is convenient to introduce the reduced variables

$$\eta \equiv p/r, \quad \xi \equiv r/R, \quad \sigma \equiv R_c/R, \tag{3.24}$$

which satisfy the inequalities

$$0 \leq \eta, \quad \xi \leq 1, \quad 0 \leq \sigma < 1. \tag{3.25}$$

We obtain

$$A^-(\xi,\eta) = \int_{y_0}^{\xi} dy\, y^{-n+1} \Big/ \sqrt{y^2-\xi^2\eta^2} \Big/ \int_\sigma^\xi dy\, y^{-n}, \tag{3.26}$$

where $y_0 = \max(\sigma, \eta\xi)$. The expression for $A^+(\xi,\eta)$ is obtained by replacing σ by unity, which implies $y_0 = 1$. For $n = 0, 2, 3$ we find

$$A_0^-(\xi,\eta) = \frac{\sqrt{y_0^2-\eta^2\xi^2} - \xi\sqrt{1-\eta^2}}{\sigma-\xi} \tag{3.27}$$

$$A_2^-(\xi,\eta) = \frac{\cos^{-1}(\eta\xi/y_0) - \cos^{-1}(\eta)}{\eta - \eta\xi/\sigma} \tag{3.28}$$

$$A_3^-(\xi,\eta) = 2\sigma^2 \frac{\sqrt{1-\eta^2\xi^2/y_0^2} - \sqrt{1-\eta^2}}{\eta^2(\sigma^2-\xi^2)}. \tag{3.29}$$

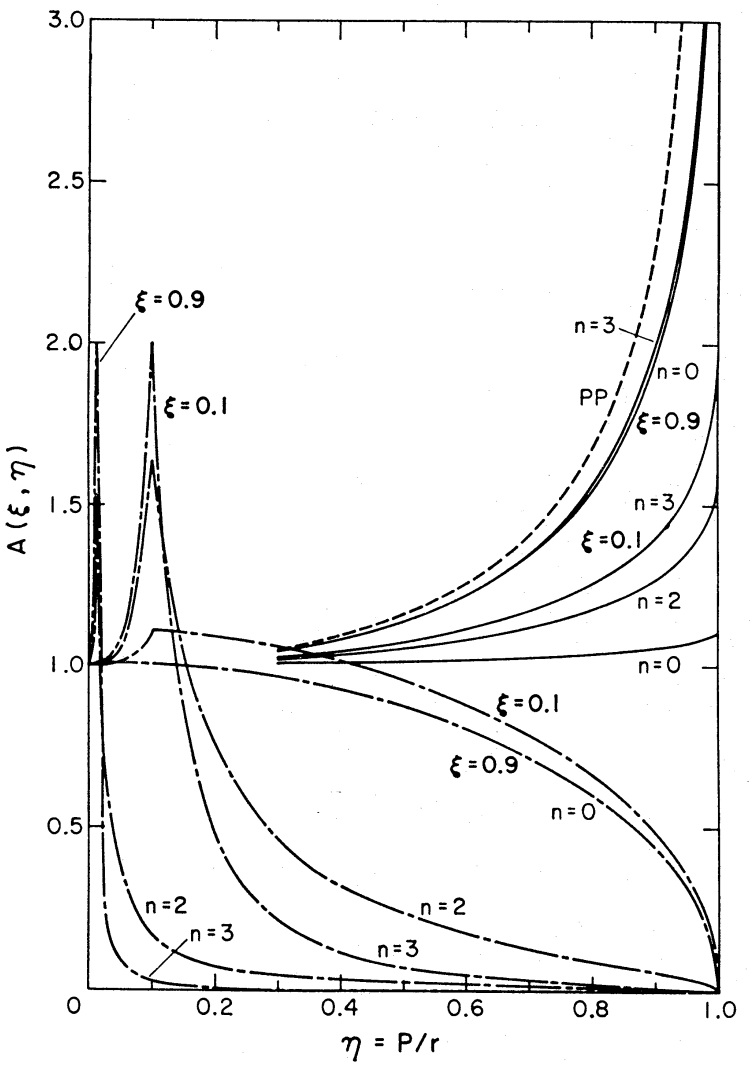

FIG. 1. *Obliquity factors for* $n = 0, 2, 3$. *Here* $\eta = p/r$, $\xi = r/R$ *and* $\sigma \equiv R_c/R = 0{\cdot}01$. ————: A^+, – – – –: A^-, ...: A (*plane parallel*).

The corresponding expressions for A^+ (with $\sigma = y_0 = 1$) become indeterminate as $\xi \to 1$. It is easy to show that

$$A_n^+(1, \eta) = 1/\sqrt{1-\eta^2}, \quad n = 0, 2, 3, \ldots . \tag{3·30}$$

The functions $A^{\pm}(\xi, \eta)$ are plotted in Fig. 1 for $\sigma = 0{\cdot}01$.

3.1.2 *Asymptotic forms for Doppler broadening.* Let us now consider the specific case of the Doppler profile $\phi(x) = (1/\sqrt{\pi})\, e^{-x^2}$ and examine the asymptotic behaviour of the escape probability as τ grows large. In this case we have, from Avrett & Hummer (1965), the asymptotic result

$$M_2(t) \sim \frac{1}{t\sqrt{\ln (t/\sqrt{\pi})}} [1 - 0{\cdot}28(\ln (t/\sqrt{\pi})^{-1} + \ldots]. \tag{3·31}$$

When $1 \ll \tau \ll T$, the second term in the expression for $P(\tau)$ is negligible compared to the first, and we have

$$P(\tau) \sim \tfrac{1}{2} \frac{1}{\tau\sqrt{\ln \tau/\sqrt{\pi}}} \int_0^r \frac{p\, dp}{r\sqrt{r^2-p^2}} \frac{1}{A(r, p)}, \tag{3·32}$$

where we have dropped the superscript + from A^+. We have also set A to its minimum value of unity in the logarithmic term. Thus, strictly speaking, the expression on the right side of (3.32) is a close upper bound on the single-flight escape probability through the surface at $\tau = 0$. By introducing the asymptotic form of the corresponding escape probability for a plane-parallel atmosphere of thickness $2T$,

$$P_{\rm pl}(\tau) \sim \frac{1}{4\tau}\frac{1}{\sqrt{\ln \tau/\sqrt{\pi}}}, \tag{3.33}$$

we can write our result as

$$P(\tau) = P_{\rm pl}(\tau)\, Q(r), \tag{3.34}$$

where

$$Q(r) \equiv 2\int_0^r \frac{p\, dp}{r\sqrt{r^2-p^2}}\frac{1}{A(r,p)}. \tag{3.35}$$

Since $A(r, p)$ is a function only of η and ξ, by rewriting (3.35) as

$$Q(\xi) = 2\int_0^1 \frac{\eta\, d\eta}{\sqrt{1-\eta^2}}\frac{1}{A(\xi,\eta)}, \tag{3.36}$$

we see that $Q(\xi)$ depends only on r/R and not on R itself. Thus the outer radius is involved in $P(\tau)$ only through the relation between r and τ. Substituting $A = 1/\sqrt{1-\eta^2}$, we find $Q(r) = 1$ in the plane-parallel case, as expected.

Since in general, for spherical symmetry, $A(\xi, \eta) \geq 1$, we find that

$$Q(\xi) \leq 2. \tag{3.37}$$

On the other hand, we find directly from the inequality (3.21) that

$$Q(\xi) \geq 1. \tag{3.38}$$

It is quite easy to show that, at the surface, $Q(r = R) = 1$ for power law opacities ($n \neq 1$) and, at the centre, $Q(0) = 2$ for the homogeneous sphere,

$$Q(0) = {\rm Cin}(\pi) = 1{\cdot}6482775\ldots$$

(Abramowitz & Stegun 1964) for $n = 2$ and $Q(0) = 1{\cdot}5$ for $n = 3$.

When $\tau = T$, both terms in (3.18) contribute equally, so that (3.32) must be doubled. However, as the same is true of (3.33), at depth $\tau = T$ in a slab of thickness $2T$, the result (3.34) is unchanged.

3.1.3 *Asymptotic form for Lorentz broadening*. In this case

$$\phi(x) = \frac{1}{\pi}\frac{1}{1+x^2} \tag{3.39}$$

and

$$M_2(t) \sim t^{-1/2}\left[1-\frac{\pi}{4t}+\frac{9\pi^2}{32t^2}+\ldots\right]. \tag{3.40}$$

Thus, when $1 \ll \tau \ll T$, we have

$$P(\tau) \sim \tfrac{1}{2}\tau^{-1/2}\int_0^r \frac{p\, dp}{r\sqrt{r^2-p^2}}\left[\frac{1}{A(r,p)}\right]^{1/2}. \tag{3.41}$$

Since the corresponding plane-parallel result is

$$P_{\rm pl}(\tau) = \tfrac{1}{3}\tau^{-1/2}, \tag{3.42}$$

we have

$$P(\tau) = P_{\rm pl}(\tau)\, Q(\xi), \tag{3·43}$$

where we can write $Q(\xi)$ in the form

$$Q(\xi) = \frac{3}{2}\int_0^1 \frac{\eta\, d\eta}{\sqrt{1-\eta^2}}\left[\frac{1}{A(\xi,\eta)}\right]^{1/2}. \tag{3·44}$$

In the same way as for the Doppler profile, we can establish the limits

$$1 \le Q(\xi) \le 3/2, \tag{3·45}$$

where the lower limit is actually achieved at $r = R$ for all opacities and the upper limit is achieved at $r = 0$ in the homogeneous sphere. For $n = 2$ we have

$$\begin{aligned} Q(0) &= \frac{3}{2}\left\{1 - \frac{1}{4}\left(\frac{1}{3}\right) - \frac{1\cdot 3}{4\cdot 8}\left(\frac{1}{5}\right) - \frac{1\cdot 3\cdot 5}{4\cdot 8\cdot 12}\left(\frac{1}{7}\right) - \dots\right\} \\ &= 1{\cdot}335\dots, \end{aligned} \tag{3·46}$$

and for $n = 3$,

$$Q(0) = 2 - \frac{1}{\sqrt{2}} = 1{\cdot}292893\dots. \tag{3·47}$$

3.1.4 *The homogeneous sphere.* For the homogeneous sphere of optical radius T, the expression for the single-flight escape probability $P(\tau)$ can be reduced substantially:

$$P(\tau) = \tfrac{1}{2}\int_0^1 d\mu\{M_2[T(\sqrt{1-\zeta^2+\zeta^2\mu^2}-\zeta\mu)] + M_2[T(\sqrt{1-\zeta^2+\zeta^2\mu^2}+\zeta\mu)]\}, \tag{3·48}$$

where

$$\zeta = \frac{r}{R} = 1 - \tau/T. \tag{3·49}$$

At the centre of the sphere $\zeta = 0$ and

$$P(\tau = T) = M_2(T). \tag{3·50}$$

From (3.1) we know that the corresponding probability of escape from the midplane of a slab of thickness $2T$ is $K_2(T)$, so that the ratio of escape probabilities is

$$P(\tau = T)/P_{\rm pl}(\tau = T) = M_2(T)/K_2(T). \tag{3·51}$$

TABLE I

Single-flight escape probabilities $P(\tau)$ for a homogeneous sphere of optical radius T

τ/T	$T = 10$	$T = 100$	$T = 1000$
0	5·85−1	5·11−1	5·02−1
0·02	4·70−1	1·31−1	7·69−3
0·04	4·05−1	6·34−2	3·68−3
0·06	3·58−1	3·92−2	2·46−3
0·08	3·21−1	2·81−2	1·88−3
0·10	2·91−1	2·20−2	1·53−3
0·20	1·96−1	1·14−2	8·65−4
0·50	1·02−1	6·01−3	4·77−4
0·70	8·35−2	5·15−3	4·13−4
1·00	7·58−2	4·78−3	3·85−4
$P(0)/P_{\rm pl}(0)$	1·15	1·02	1·00
$P(T)/P_{\rm pl}(T)$	2·28	2·11	2·07

This ratio is unity for $T = 0$, reaches a maximum of about 2·35 near $T = 6$ for Doppler broadening and falls off slowly to 2 as $T \to \infty$. For the Lorentz profile, this ratio reaches a maximum of about 1·59 near $T = 7{\cdot}5$ and asymptotically approaches 3/2.

In Table I, values of $P(\tau)$ are given for $T = 10$, 10^2 and 10^3 for Doppler broadening. The ratio of $P(\tau)$ to the single-flight escape probability $P_{\rm pl}(\tau)$ for a slab of thickness $2T$ increases monotonically with τ between the values in the last two lines of Table I. Thus even the non-asymptotic region, $P(\tau)$ exceeds $P_{\rm pl}(\tau)$ by a factor only slightly larger than $Q(0)$.

3.1.5 *Mean number of scatterings and mean escape probabilities.* These two quantities are useful in characterizing the net effect of scattering in the transfer process. The mean number of scatterings is simply the ratio of the number of photons *emitted* to the number of photons *created* per unit time in the medium, while the mean escape probability is the ratio of the number of photons escaping from the medium per unit time to the number created. For spherical systems

$$\langle N\rangle = \int_{R_c}^{R} dr\, r^2 k(r)\, S(r) \Big/ \int_{R_c}^{R} dr\, r^2 k(r)\, \epsilon(r)\, B(r) \qquad (3{\cdot}52)$$

and

$$\langle P\rangle = \int_{R_c}^{R} dr\, r^2 k(r)\, S(r)\, P(r) \Big/ \int_{R_c}^{R} dr\, r^2 k(r)\, \epsilon(r)\, B(r), \qquad (3{\cdot}53)$$

where $P(r)$ is the single-flight escape probability from radius r. For plane-parallel systems similar expressions hold with the r^2 factors removed.

It is important to stress that, in contrast to the single-flight escape probability which depends only on the geometrical and constitutive properties of the system, $\langle N\rangle$ and $\langle P\rangle$ depend on the source function and can be evaluated only after the transfer problem has been solved. While $\langle N\rangle$ and $\langle P\rangle$ are often thought of as having some sort of reciprocal relation, it is clear that any relation of this kind must depend on the source function, which in turn depends on $P(\tau)$ in a complicated way.

Another difficulty of interpretation arises when one compares $\langle N\rangle$ or $\langle P\rangle$ for spherical systems to the corresponding quantity in the plane-parallel case. For example, let us consider the homogeneous sphere of optical radius T and a slab of thickness $2T$. Holding ϵ, B and k fixed, we can easily show that

$$\langle P\rangle/\langle P\rangle_{\rm pl} = 3\int_0^1 d\zeta\, \zeta^2 S(\zeta)\, P(\zeta) \Big/ \int_0^1 d\zeta\, S_{\rm pl}(\zeta)\, P_{\rm pl}(\zeta), \qquad (3{\cdot}54)$$

where ζ is the ratio of the optical distance from the centre of the system to T; a similar relation holds for $\langle N\rangle/\langle N\rangle_{\rm pl}$. When $P/P_{\rm pl}$ is known from arguments given above, it is difficult to say anything about $\langle P\rangle/\langle P\rangle_{\rm pl}$ because of the weight factor ζ^2. Even if $S = \text{const.} \times S_{\rm pl}$, the factor ζ^2 causes $\langle N\rangle/\langle N\rangle_{\rm pl}$ to depend strongly on the shape of $S_{\rm pl}$. We shall see that our arguments concerning $P/P_{\rm pl}$ make it possible to predict $S/S_{\rm pl}$, but give very little information about $\langle P\rangle/\langle P\rangle_{\rm pl}$ or $\langle N\rangle/\langle N\rangle_{\rm pl}$.

For the special case of a homogeneous sphere and a homogeneous slab of optical radius and semi-thickness T, respectively, with ' a uniform distribution of emitters ', and no absorption, Capriotti (1965) derives expressions for $\langle P\rangle$ and $\langle P\rangle_{\rm pl}$, and shows that $\lim_{T\to\infty} \langle P\rangle/\langle P\rangle_{\rm pl} = 3$. The significance of this result is not clear.

3.2 *Bias in scattering to larger radii*

Although we are assuming that the scattering of radiation is isotropic, it is a fundamental property of spherical systems that a photon scattered from a certain radius ends its flight at a larger radius more often than at a smaller one. This behaviour is quite different from the situation in plane-parallel geometries in which a photon goes with equal probabilities to larger or smaller depths. In the plane-parallel case, the kernel of the integral equation for the source function depends only on the absolute difference of the optical depths of the initial and final points, while in the spherical case, the most that can be said is that $rS(r)$ satisfies an integral equation with optical depth as the independent variable whose kernel is a symmetric function of the initial and final radii. In the special case of a homogeneous sphere, this kernel depends only on the absolute difference of the initial and final radii (see Appendix I). Even in this case, as we shall see, a bias towards larger radii exists.

It is unnecessary for this purpose to consider the single-scattering kernel. Instead, following the suggestion by Dr G. B. Rybicki, we can easily derive a relatively simple expression for the probability that a photon emitted at radius r ends its flight (i.e. experiences its next encounter with an atom) at some radius less than r. If we denote this probability by $w_1(r)$, then the probability that the photon ends its flight at a larger radius or escapes the atmosphere is clearly $w_2(r) = 1 - w_1(r)$, and the ratio of $w_2(r)$ to $w_1(r)$ expresses the bias at radius r for scattering towards a larger radius.

Consider a point on a sphere of radius r interior to, and concentric with, the spherical system. For simplicity we ignore the central cavity. If $2\tau_0(\theta)$ is the mean optical depth along a chord from the point in question, making an angle θ with the radius vector to the point, then the probability that a photon emitted with the probability distribution $\phi(x)$ ends its path within the sphere is

$$\begin{aligned} w_1(r) &= \tfrac{1}{2}\int_{-\infty}^{\infty} dx\,\phi(x)\int_0^{\pi/2} d\theta\,\sin\theta\int_0^{2\tau_0(\theta)} d\tau\,\phi(x)\,e^{-\tau\phi(x)} \\ &= \tfrac{1}{2}\int_{-\infty}^{\infty} dx\,\phi(x)\int_0^{\pi/2} d\theta\,\sin\theta\,[1-e^{-2\tau_0(\theta)\,\phi(x)}] \qquad (3\cdot55) \\ &= \tfrac{1}{2}\left[1-\int_0^{\pi/2} d\theta\,\sin\theta M_2(2\tau_0(\theta))\right]. \end{aligned}$$

For power law opacities written in the form (3.7), it is readily shown that

$$\tau_0(\theta) = \begin{cases} Kr\cos\theta, & n=0 \\ Kr^{-1}(\pi/2-\theta)\csc(\theta), & n=2 \\ Kr^{-2}\cos\theta\csc^2\theta, & n=3. \end{cases} \qquad (3\cdot56)$$

The ratio $\rho(r) \equiv w_2(r)/w_1(r)$ turns out to depend only on the parameter

$$\gamma = 2Kr^{1-n}, \quad n = 0, 2, 3, \qquad (3\cdot57)$$

where

$$K = T\Big/\int_{Rc}^{R} r^{-n}\,dr. \qquad (3\cdot58)$$

As $r \to 0$, $\rho \to \infty$. In Table II, values of ρ are given as a function of γ for $n = 0, 2, 3$.

TABLE II

The ratio ρ of the probability of outward scattering to the probability of inward scattering as a function of the parameter γ defined in equation (3.57)

γ	$n=0$	$n=2$	$n=3$
$1-1$	$1\cdot01+2$	$4\cdot53+1$	$2\cdot68+1$
$2-1$	$5\cdot07+1$	$2\cdot42+1$	$1\cdot59+1$
$5-1$	$2\cdot06+1$	$1\cdot10+1$	$8\cdot30$
1	$1\cdot06+1$	$6\cdot37$	$5\cdot25$
2	$5\cdot64$	$3\cdot90$	$3\cdot45$
5	$2\cdot73$	$2\cdot28$	$2\cdot16$
$1+1$	$1\cdot82$	$1\cdot68$	$1\cdot64$
$2+1$	$1\cdot41$	$1\cdot36$	$1\cdot35$
$5+1$	$1\cdot17$	$1\cdot16$	$1\cdot15$
$1+2$	$1\cdot09$	$1\cdot08$	$1\cdot08$
$2+2$	$1\cdot05$	$1\cdot04$	$1\cdot04$
$5+2$	$1\cdot02$	$1\cdot02$	$1\cdot02$
$1+3$	$1\cdot01$	$1\cdot01$	$1\cdot01$

For a homogeneous sphere ($R_c = 0$), $\gamma = 2Tr/R$, so that the bias is large only when $r \ll R$ or when T is not too large. If the central cavity has a non-zero radius R_c, then our result is accurate only for $r \gg R_c$, since the effect of the cavity was neglected. Thus, for the homogeneous shell, we must have $R \geq r \gg R_c$, in which we obtain the same results as for the homogeneous sphere. For $n = 2$ and 3, when $R > r \gg R_c$, we have

$$\gamma = 2(n-1)\, Tr^{1-n}\,(R_c R)^{n-1}\,(R^{n-1} - R_c{}^{n-1})^{-1} \sim 2(n-1)\, T(R_c/r)^{n-1},$$

so that $\rho(\gamma)$ is large when r is large or T is small. For $T = 1000$, $R = 300$, $R_c = 1$, $r = 150$, we have $\rho_0 \simeq 1\cdot01$, $\rho_2 \simeq 1\cdot5$, $\rho_3 \simeq 17$. Thus when $n = 0$ the bias is most important in the inner regions, i.e. throughout a relatively small fraction of the atmosphere, while for $n \geq 2$, the bias is largest in the outer regions, comprising the larger portion of the atmosphere.

The reason for this strong dependence on n is readily seen, for when the opacity decreases outward, the photon's mean free path in the outward direction can be substantially longer than in the inward direction. In Fig. 2 we have plotted for $n = 2$ and 3 the loci of points lying one monochromatic mean free path away from source points whose radii R_1 are shown in the figure; the corresponding frequencies are given in the caption. From the figure it is apparent that the bias is particularly important for long mean free paths.

While the quantitative importance of this effect will be discussed below, a remark on one aspect of its significance is appropriate. In the plane-parallel situation, for scattering with complete redistribution, a photon created near the centre of the line will typically not move far from its point of creation as it is repeatedly scattered, and finally escapes from the atmosphere in one long flight. This circumstance, which has been discussed in detail by Rybicki & Hummer (1969), provides the theoretical basis for the on-the-spot or escape-probability methods. In principle, the bias discussed above for spherical systems will tend to increase the outward drift of photons as they are scattered and will diminish the importance of the final longest flight. Consequently, the escape probability method will be less reliable than for plane-parallel systems.

3.3 *Dilution and the large-R limit*

The behaviour of the radiation field from a discrete, spherical source of non-zero

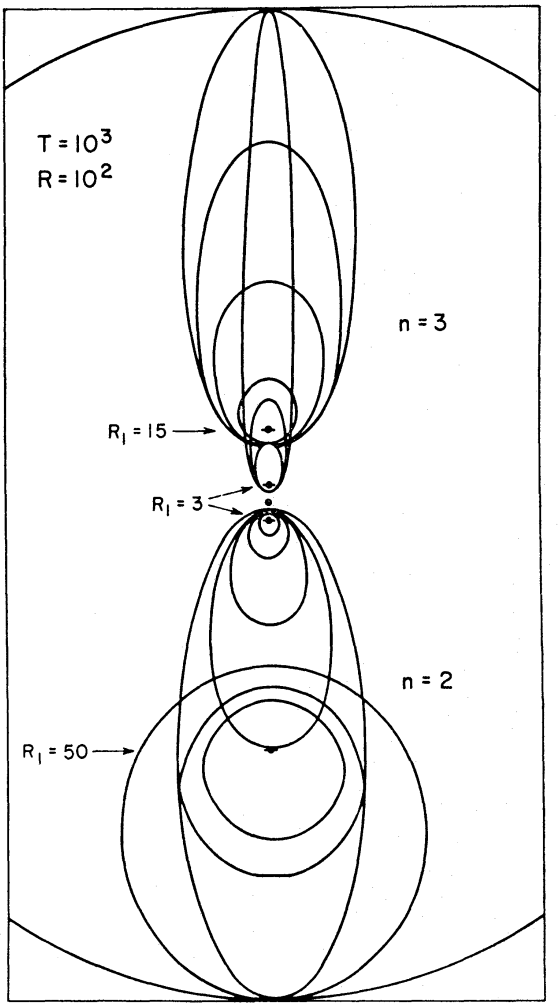

FIG. 2. *Loci of points one monochromatic mean free path from points at indicated values of radius r_1 in atmospheres with $R = 10^2$, $T = 10^3$ and $n = 2$ (bottom half) and $n = 3$ (top half). For $n = 2$, the frequencies associated with loci around $r_1 = 3$ are $x = 2{\cdot}179$, $2{\cdot}226$, $2{\cdot}263$, $2{\cdot}277$, $2{\cdot}284$ and around $r_1 = 50$ are $x = 1{\cdot}048$, $1{\cdot}155$, $2{\cdot}011$. For $n = 3$, the frequencies at $r_1 = 3$ are $x = 2{\cdot}020$, $2{\cdot}029$, $2{\cdot}034$ and at $r_1 = 15$ are $x = 0{\cdot}691$, $0{\cdot}895$, $0{\cdot}936$, $0{\cdot}947$.*

radius in a vacuum is particularly simple, and depends only on the spectral and angular distribution of the radiation emerging from the source. We shall use the term *dilution* to refer to the modification of a radiation field as it flows from a smaller to a larger region of space without interacting significantly with the gas. It seems logical that certain simplifications should appear in our models when a substantial fraction of the atmosphere is optically thin at all frequencies. It is also of interest to inquire into the behaviour of the radiation field at a given frequency in those parts of the atmosphere in which the monochromatic optical depth is much less than unity.

For spherical atmospheres of fixed optical thickness T in which $k(r)$ decreases as r increases, it is clear that when R becomes sufficiently large, a substantial portion of the atmosphere will be optically thin at all frequencies. To make things definite, let us consider power law opacities ($n > 1$) and calculate the radius r_1 at which $\tau = 1$. From the expression

$$\tau(r) = T(r^{-n+1} - R^{-n+1})/(R_c^{-n+1} - R^{-n+1}) \qquad (3{\cdot}59)$$

we readily obtain

$$r_1/R = T^{1/n-1}/[T-1+(R/R_c)^{n-1}]^{1/n-1} \underset{R\gg R_c}{\sim} T^{1/n-1}R_c/[R^{n-1}+TR_c{}^{n-1}]^{1/n-1}. \quad (3.60)$$

Thus as $R\to\infty$, with T fixed, the radius at which $\tau = 1$ approaches a limiting value of $r_1 = TR_c$ for $n = 2$ and $r_1 = T^{1/2}R_c$ for $n = 3$. More generally, when R is sufficiently large, the $\tau(r)$ relation for $\tau > 1$ or $r < r_1$ becomes essentially independent of R, as does the radiation field.

It is convenient to have a measure of the outer radius R that defines the large-R regime discussed in the preceding paragraph. Following the suggestion of Dr J. I. Castor, we let R_t be the value of R for which $\tau = 1$ occurs midway between the inner and outer boundaries, i.e. $r_1 = \frac{1}{2}(R-R_c)$. From (3.59) or from (3.60), we find that

$$R_t/R_c = T^{1/n-1}[(\tfrac{1}{2})^{-n+1}-1]^{1/n-1}, \quad n\geq 2. \quad (3.61)$$

In particular, we have

$$R_t/R_c = \begin{cases} T, & n = 2, \\ \sqrt{3}T^{1/2}, & n = 3. \end{cases} \quad (3.62)$$

Thus, when $R\gg R_t$, the transfer problem is essentially independent of R in the region $r < r_1$ and has a simple form for $r\gg r_1$.

The radius $r_1(x)$ at which the monochromatic optical depth is unity for frequency x is also useful in understanding the behaviour of the radiation field. For $r\ll r_1(x)$, the intensity with frequency x will be essentially isotropic and its dependence on radius will be determined by the radiation field in all frequencies. For $r\gg r_1(x)$, the intensity will be strongly forward peaked and J_x and H_x will be decreasing roughly as r^{-2}, although if the atmosphere is still optically thick at frequencies closer to line centre, scattering from these frequencies may cause significant deviations from the r^{-2} behaviour.

A measure of the effect of dilution at frequency x is provided by the ratio

$$\mathscr{E}_x \equiv R/r_1(x). \quad (3.63)$$

If this quantity is of order unity, dilution will play only a small role in establishing the radiation field at frequency x. If $\mathscr{E}_x$ is large, dilution is important, and the angular width of the forward peaked radiation is roughly $\mathscr{E}_x{}^{-1}$.

4. INTERPRETATION OF NUMERICAL RESULTS

While the variable Eddington factor method outlined in Section 2 is capable of handling arbitrary radial variations in $k(r)$, ϵ, and B, we shall limit our discussion here to very simple and highly idealized problems in which the great generality of the method is not used. Our emphasis will be on identifying and understanding the basic features of line formation in spherical systems. Because we wish to use the familiar results for the isothermal plane-parallel configurations as reference points, we consider mainly spherical shells of outer radius R and optical thickness T surrounding a hollow central cavity of radius R_c, and study the behaviour of the radiation field as R increases from $R = R_c$, the plane-parallel limit. We take $R_c = 1$ as our unit of length for all shell models. We have used the opacity laws $k(r) = Kr^{-n}$, $n = 0, 2, 3$. Since the hollow core is equivalent to a reflecting boundary, in the plane-parallel limit the shell model is equivalent to a slab of optical thickness $2T$, with symmetry about its midplane.

The simplest plane-parallel atmospheres are those in which ϵ and B are constant. When spherical atmospheres are considered, two natural generalizations appear. In the first of these, ϵ and B are held constant, so that the rate at which photons are created in the shell $r, r+dr$ is $4\pi r^2 k(r)\,\epsilon B$. This leads to a photon creation rate *per unit optical depth* $d\tau = k(r)\,dr$ that is proportional to r^2. In the second generalization (suggested to us by Dr G. B. Rybicki) we hold ϵ fixed and assume $B \propto r^{-2}$ so that the photon creation rate per unit optical depth is constant, as it is for isothermal plane-parallel cases. In the first case, the photons are created substantially closer to the surface than in the second, and escape much more readily. Most of our results have been obtained with $B = 1$.

4.1 *The homogeneous sphere*

Before going on to interpret the results of the variable Eddington factor method for spherical shells, it is instructive to consider first the simplest of all spherical configurations, the homogeneous sphere. The line transfer problem in this case can easily be solved by a simple generalization of the kernel approximation method developed by Avrett & Hummer (1965). Since only a second or two of computer time is required for each model, a wide range of parameters can be surveyed. The details are given in the Appendix. Solutions have been obtained for $B = 1$ with both Doppler and Lorentz profiles for a large range of ϵ and T values.

In Table III we give values of the source function for several typical cases (no solutions for this problem appear to have been tabulated previously). The dependence on ϵ and T are seen to be quite similar to the plane-parallel case. In Table IV values of $\langle N\rangle$ are given and compared with an asymptotic expression ($T \to \infty$) given by Ivanov (1970) for a homogeneous sphere with conservative Doppler scattering:

$$\langle N\rangle = \tfrac{3}{16}\sqrt{\pi\tau_0}\,\sqrt{\ln \tau_0}\left[1 - \frac{0{\cdot}77954}{\ln \tau_0} + o(1/\ln \tau_0)^2\right], \qquad (4.1)$$

where

$$\tau_0 = \frac{2}{\sqrt{\pi}}\,T$$

is the line centre optical *diameter* of the sphere; our parameter T is the mean optical radius. For $\epsilon = 10^{-8}$ we see that as T increases from unity, our values of $\langle N\rangle$ approach to within 2 per cent of Ivanov's at $T = 10^5$. For these values of T, $\epsilon T \ll 1$ and the scattering is essentially conservative. For larger values of T, the loss of photons by absorption starts to become important and our values of $\langle N\rangle$ fall below those of Ivanov, even though his expression becomes more accurate. Since the coefficient of $(\ln \tau_0)^{-2}$ is unknown, we cannot assess our accuracy by this comparison (for plane-parallel cases the maximum error was less than 1 per cent). Nevertheless the agreement obtained does tend to increase confidence in this calculation.

The ratio $S(\tau)/S_{\rm pl}(\tau)$ of the source functions for spheres and slabs of optical radius and semi-thickness T, respectively, was evaluated at many points throughout each model. It was found to vary monotonically with τ between the surface and centre of the atmospheres, increasing with τ for large T and decreasing for small T. The values of this ratio at $\tau = 0$ and $\tau = T$ appear in Table V along with $\langle N\rangle/\langle N\rangle_{\rm pl}$. For $T = 10^2$ and 10^3, very weak minima were seen at points inside the atmospheres, but these values differed negligibly from those at $\tau = 0$ and T. The

Table III

Source functions in homogeneous spheres with Doppler (D) and Lorentz (L) profiles, for $B = 1$ and indicated values of ϵ and the optical radius T

τ	$T = 1$		$T = 10$			$T = 10^2$				$T = 10^3$				
	$\epsilon =$ 10^{-2} D	$\epsilon =$ 10^{-2} L	$\epsilon =$ 10^{-2} D	$\epsilon =$ 10^{-4} D	$\epsilon =$ 10^{-2} L	$\epsilon =$ 10^{-2} D	$\epsilon =$ 10^{-4} D	$\epsilon =$ 10^{-2} L	$\epsilon =$ 10^{-4} L	$\epsilon =$ 10^{-2} D	$\epsilon =$ 10^{-4} D	$\epsilon =$ 10^{-6} D	$\epsilon =$ 10^{-2} L	$\epsilon =$ 10^{-4} L
0	1·19−2	1·08−2	2·51−2	2·59−4	1·53−2	6·67−2	9·20−4	2·68−2	2·77−4	9·40−2	3·18−3	3·37−5	4·47−2	4·98−4
1−1	1·27−2	1·10−2	2·75−2	2·83−4	1·58−2	7·35−2	1·02−3	2·79−2	2·89−4	1·04−1	3·51−3	3·73−5	4·65−2	5·19−4
3−1	1·34−2	1·13−2	3·08−2	3·18−4	1·66−2	8·32−2	1·16−3	2·95−2	3·05−4	1·17−1	4·00−3	4·24−5	4·91−2	5·48−4
1	1·44−2	1·16−2	3·92−2	4·07−4	1·85−2	1·09−1	1·53−3	3·34−2	3·46−4	1·54−1	5·33−3	5·65−5	5·57−2	6·23−4
3			5·51−2	5·76−4	2·17−2	1·63−1	2·35−3	4·07−2	4·23−4	2·30−1	8·21−3	8·71−5	6·80−2	7·65−4
1+1			7·44−2	7·86−4	2·52−2	2·80−1	4·28−3	5·42−2	5·69−4	3·94−1	1·53−2	1·62−4	9·12−2	1·04−3
3+1						4·39−1	7·49−3	6·99−2	7·42−4	6·11−1	2·82−2	3·00−4	1·20−1	1·38−3
1+2						5·69−1	1·10−2	8·26−2	8·86−4	8·30−1	5·43−2	5·85−4	1·58−1	1·87−3
3+2										9·30−1	9·28−2	1·02−3	1·97−1	2·40−3
1−3										9·60−1	1·32−1	1·48−3	2·26−1	2·85−3

τ	$T = 10^4$					$T = 10^6$					$T = 10^8$				
	$\epsilon =$ 10^{-2} D	$\epsilon =$ 10^{-4} D	$\epsilon =$ 10^{-6} D	$\epsilon =$ 10^{-2} L	$\epsilon =$ 10^{-4} L	$\epsilon =$ 10^{-4} D	$\epsilon =$ 10^{-6} D	$\epsilon =$ 10^{-8} D	$\epsilon =$ 10^{-2} L	$\epsilon =$ 10^{-4} L	$\epsilon =$ 10^{-6} D	$\epsilon =$ 10^{-8} D	$\epsilon =$ 10^{-2} L	$\epsilon =$ 10^{-4} L
0	9·92−2	7·44−3	1·17−4	6·63−2	8·85−4	9·94−3	7·80−4	1·31−5	9·39−2	2·70−3	9·95−4	8·02−5	9·93−2	6·61−3
1−1	1·09−1	8·22−3	1·29−4	6·90−2	9·22−4	1·10−2	8·62−4	1·45−5	9·78−2	2·82−3	1·10−3	8·87−5	1·03−1	6·89−3
3−1	1·24−1	9·36−3	1·47−4	7·29−2	9·74−4	1·25−2	9·82−4	1·65−5	1·03−1	2·98−3	1·25−3	1·01−4	1·09−1	7·28−3
1	1·63−1	1·25−2	1·96−4	8·26−2	1·11−3	1·67−2	1·31−3	2·20−5	1·17−1	3·38−3	1·67−3	1·35−4	1·24−1	8·27−3
3	2·43−1	1·92−2	3·02−4	1·01−1	1·36−3	2·57−2	2·02−3	3·40−5	1·43−1	4·15−3	2·57−3	2·08−4	1·51−1	1·02−2
1+1	4·14−1	3·58−2	5·62−4	1·35−1	1·84−3	4·78−2	3·77−3	6·33−5	1·92−1	5·63−3	4·80−3	3·87−4	2·03−1	1·38−2
3+1	6·41−1	6·61−2	1·05−3	1·78−1	2·47−3	8·83−2	7·01−3	1·18−4	2·52−1	7·53−3	8·94−3	7·21−4	2·67−1	1·84−2
1+2	8·62−1	1·29−1	2·07−3	2·36−1	3·36−3	1·72−1	1·39−2	2·34−4	3·34−1	1·03−2	1·77−2	1·43−3	3·53−1	2·51−2
3+2	9·57−1	2·27−1	3·81−3	2·97−1	4·42−3	3·02−1	2·56−2	4·32−4	4·21−1	1·36−2	3·27−2	2·64−3	4·45−1	3·32−2
1+3	9·87−1	3·90−1	7·22−3	3·72−1	5·93−3	5·14−1	4·94−2	8·36−4	5·27−1	1·83−2	6·30−2	5·11−3	5·57−1	4·48−2
3+3	9·95−1	5·66−1	1·23−2	4·39−1	7·58−3	7·33−1	8·85−2	1·51−3	6·25−1	2·41−2	1·13−1	9·23−3	6·61−1	5·89−2
1+4	9·97−1	6·85−1	1·76−2	4·86−1	8·97−3	9·04−1	1·64−1	2·86−3	7·24−1	3·24−2	2·09−1	1·75−2	7·65−1	7·93−2
3+4						9·68−1	2·77−1	5·08−3	7·97−1	4·23−2	3·51−1	3·13−2	8·41−1	1·04−1
1+5						9·90−1	4·53−1	9·36−3	8·55−1	5·62−2	5·68−1	5·85−2	9·02−1	1·39−1
3+5						9·96−1	6·27−1	1·56−2	8·91−1	7·11−2	7·76−1	1·03−1	9·38−1	1·80−1
1+6						9·97−1	7·37−1	2·21−2	9·09−1	8·34−2	9·22−1	1·86−1	9·62−1	2·35−1
3+6											9·74−1	3·09−1	9·75−1	2·96−1
1+7											9·91−1	4·93−1	9·84−1	3·70−1
3+7											9·96−1	6·67−1	9·88−1	4·37−1
1+8											9·98−1	7·70−1	9·90−1	4·84−1

TABLE IV

Kernel approximation estimates of $\langle N \rangle$ for the homogeneous sphere

	Doppler						Ivanov	Lorentz	
log T/log ϵ	−2	−3	−4	−5	−6	−7	−8	($\epsilon = 0$)	−2	−4
0	1·31	1·32	1·32	1·32	1·32	1·32	1·32		1·12	1·12
1	4·88	5·07	5·09	5·10	5·10	5·10	5·10	3·96	2·03	2·05
2	3·64+1	5·77+1	6·14+1	6·18+1	6·19+1	6·19+1	6·19+1	6·81+1	6·20	6·56
3	8·44+1	4·26+2	7·56+2	8·22+2	8·30+2	8·30+2	8·30+2	8·84+2	1·76+1	2·13+1
4	9·78+1	8·67+2	4·73−3	9·08+3	1·00+4	1·02+4	1·02+4	1·05+4	4·00+1	6·72+1
5		9·81+2	8·82+3	5·06+4	1·03+5	1·16+5	1·17+5	1·19+5	6·73+1	2·10+2
6			9·83+3	8·92+4	5·31+5	1·13+6	1·28+6	1·32+6	8·63+1	6·33+2
7				9·84+4	8·99+5	5·51+6	1·22+7	1·44+7		1·75+3
8					9·86+5	9·06+6	5·68+7	1·55+8		3·98+3
9						9·86+6	9·10+7	1·65+0		6·71+3
10							9·87+7	1·74+10		8·62+3

Table V

Comparison of the source functions at $\tau = 0$ and $\tau = T$, and the mean number of scatterings for homogeneous spheres and slabs of optical radius and semi-thickness T, respectively

	Doppler $\epsilon = 10^{-2}$			Doppler $\epsilon = 10^{-4}$			Doppler $\epsilon = 10^{-6}$		
log T	$S/S_{pl}(0)$	$S/S_{pl}(T)$	$\langle N\rangle/\langle N\rangle_{pl}$	$S/S_{pl}(0)$	$S/S_{pl}(T)$	$\langle N\rangle/\langle N\rangle_{pl}$	$S/S_{pl}(0)$	$S/S_{pl}(T)$	$\langle N\rangle/\langle N\rangle_{pl}$
0	0·67	0·64	0·62	0·67	0·63	0·62	0·67	0·63	0·62
1	0·52	0·50	0·40	0·49	0·46	0·37	0·49	0·46	0·37
2	0·72	0·76	0·59	0·47	0·47	0·34	0·47	0·47	0·34
3	0·95	0·98	0·90	0·54	0·55	0·40	0·48	0·48	0·35
4	0·99	1·00	0·99	0·78	0·83	0·67	0·49	0·49	0·36
5				0·96	0·98	0·93	0·56	0·57	0·43
6				0·99	1·00	0·99	0·81	0·86	0·71
7							0·97	0·99	0·94
8							1·00	1·00	0·99

	Doppler $\epsilon = 10^{-8}$			Lorentz $\epsilon = 10^{-2}$			Lorentz $\epsilon = 10^{-4}$		
log T	$S/S_{pl}(0)$	$S/S_{pl}(T)$	$\langle N\rangle/\langle N\rangle_{pl}$	$S/S_{pl}(0)$	$S/S_{pl}(T)$	$\langle N\rangle/\langle N\rangle_{pl}$	$S/S_{pl}(0)$	$S/S_{pl}(T)$	$\langle N\rangle/\langle N\rangle_{pl}$
0	0·67	0·63	0·62	0·81	0·79	0·78	0·81	0·79	0·78
1	0·49	0·46	0·37	0·67	0·65	0·59	0·67	0·64	0·58
2	0·49	0·47	0·34	0·69	0·69	0·59	0·66	0·66	0·56
3	0·48	0·48	0·35	0·73	0·74	0·65	0·67	0·67	0·57
4	0·48	0·49	0·36	0·82	0·83	0·74	0·67	0·67	0·57
5	0·49	0·49	0·36	0·90	0·92	0·86	0·68	0·68	0·58
6	0·50	0·50	0·37	0·96	0·97	0·94	0·69	0·69	0·60
7	0·58	0·59	0·45				0·73	0·74	0·65
8	0·83	0·88	0·73				0·81	0·83	0·74
9	0·97	0·99	0·95				0·90	0·92	0·86
10	1·00	1·00	0·99				0·96	0·97	0·94

constancy of the ratio $S(\tau)/S_{\rm pl}(\tau)$ for a given ϵ and T is remarkable and supports the argument in the Introduction that homogeneous spheres do not fully develop the characteristics of spherical systems. We also observe that $S(\tau)$ falls below $S_{\rm pl}(\tau)$ by a factor only slightly larger than two (or 3/2 for the Lorentz case), in accordance with the increase in the single-flight escape probability predicted in Section 3.1. On the other hand $\langle N\rangle/\langle N\rangle_{\rm pl}$ is seen to become as small as 1/3 for the Doppler case and 0·56 (probably 0·50 if a finer grid of results were available) for the Lorentz case. This illustrates the importance of the $(r/R)^2$ weight factor discussed in Section 3.1.5. The relation of this result with that of Capriotti (1965) for $\langle P\rangle/\langle P\rangle_{\rm pl}$, mentioned in Section 3.1.5, is unclear and, in view of the discussion of that section, may be fortuitous.

4.2 *Source function for spherical shells*

Since we are interested more in the general features of the transfer process in spherical shells than in the details of any particular model, we shall, in this section, examine several sequences of source functions for power law opacities. In Section 4.3, the details of the radiation field for the case $n = 2$ are discussed.

4.2.1 *Models with* $B = 1$. In Figs 3, 4 and 5 we plot log S *vs.* log τ for $n = 0$, 2, 3 respectively. In all cases $T = 10^3$, $B = 1$ and $R_c = 1$. In each figure we show

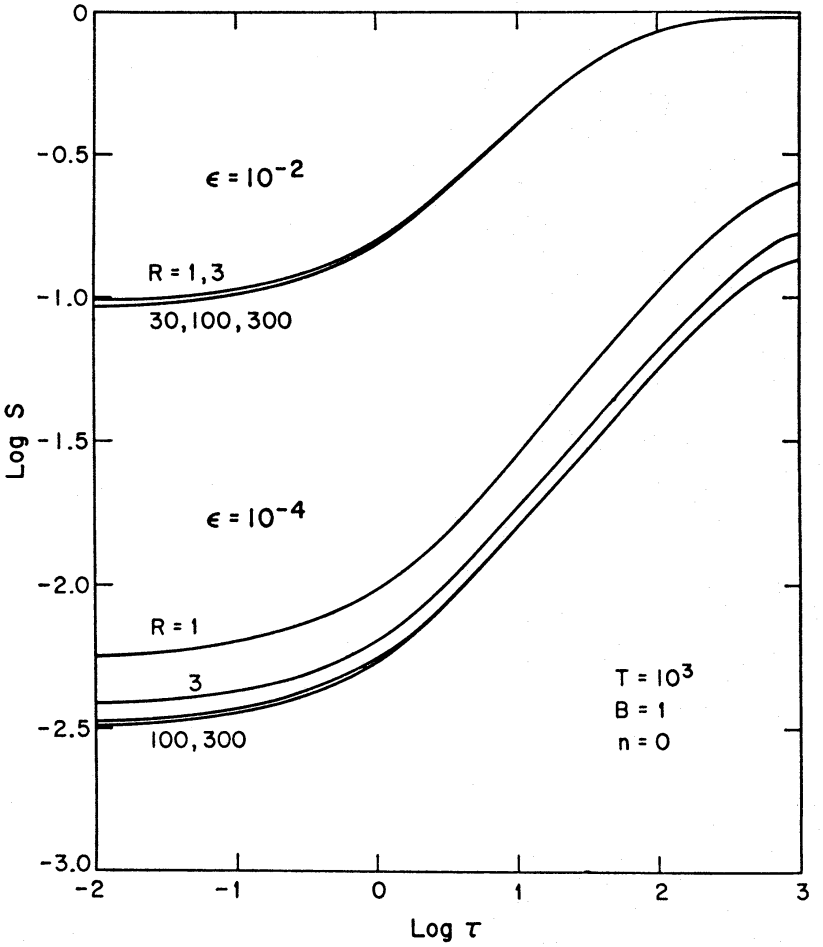

FIG. 3. *Source function vs. optical depth in an atmosphere with* $T = 10^3$, $B = 1$ *and a constant opacity. The radius of inner boundary is* $R_c = 1$ *and the radius of outer boundary R labels curves.*

two sequences of curves with $\epsilon = 10^{-2}$ and 10^{-4}. In the first of these $\epsilon T \gg 1$ and at least in the plane-parallel limit the atmospheres are effectively thick, i.e. most of the photons are absorbed before escaping, while in the second, $\epsilon T \ll 1$ and the atmospheres are effectively thin, i.e. most photons escape. The curves are labelled by the value of the outer radius R; those labelled $R = 1$ are for plane-parallel models of thickness $2T$.

In the case $n = 0$, the maximum deviation of the source function from the plane-parallel result is about a factor two, in accordance with the results for the

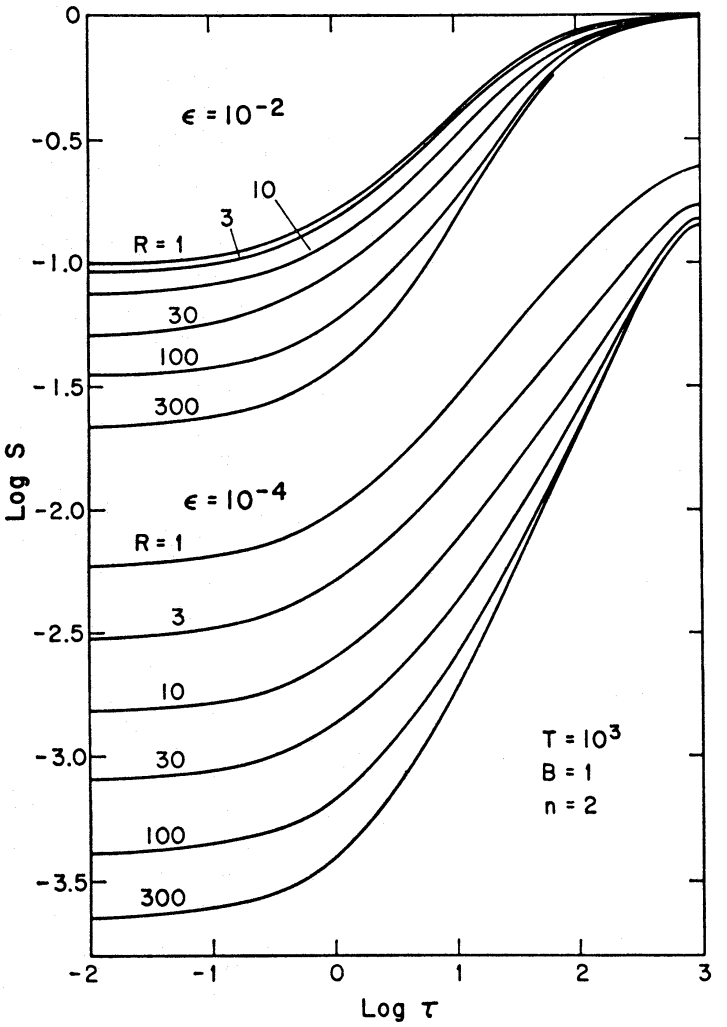

FIG. 4. *Source function vs. optical depth in an atmosphere with* $T = 10^3$, $B = 1$ *and* $k(r) = Kr^{-2}$. *The radius of inner boundary is* $R_c = 1$ *and the radius R of outer boundary labels curves.*

homogeneous sphere and the mean-escape probability arguments. The source functions for $R = 300$ are in substantial agreement with the kernel-approximation results for the homogeneous sphere. We see that R does not have to be very large for the effect of the central cavity to become unimportant, particularly when $\epsilon = 10^{-2}$.

For $n = 2$, as R increases from 1 to 300, the source functions depart very substantially from the plane-parallel limit; for $\epsilon = 10^{-4}$ the maximum deviation is about $1\frac{1}{2}$ orders of magnitude. Since with $B = 1$ the minimum value of the source function is ϵ, somewhat smaller values of the source function can occur for

larger values of R. In terms of the discussion of Section 3.3, all values of R considered here are smaller than $R_t = T = 10^3$.

When $\epsilon = 10^{-2}$, S goes to B as τ approaches T for all values of R considered here, and since the curves seem to be approaching a limiting curve at large τ, this behaviour should persist as $R \to \infty$. In other words, the effects of a large spherical extension will not modify the saturation properties of the medium, except possibly in marginal cases which are barely saturated in the plane-parallel limit.

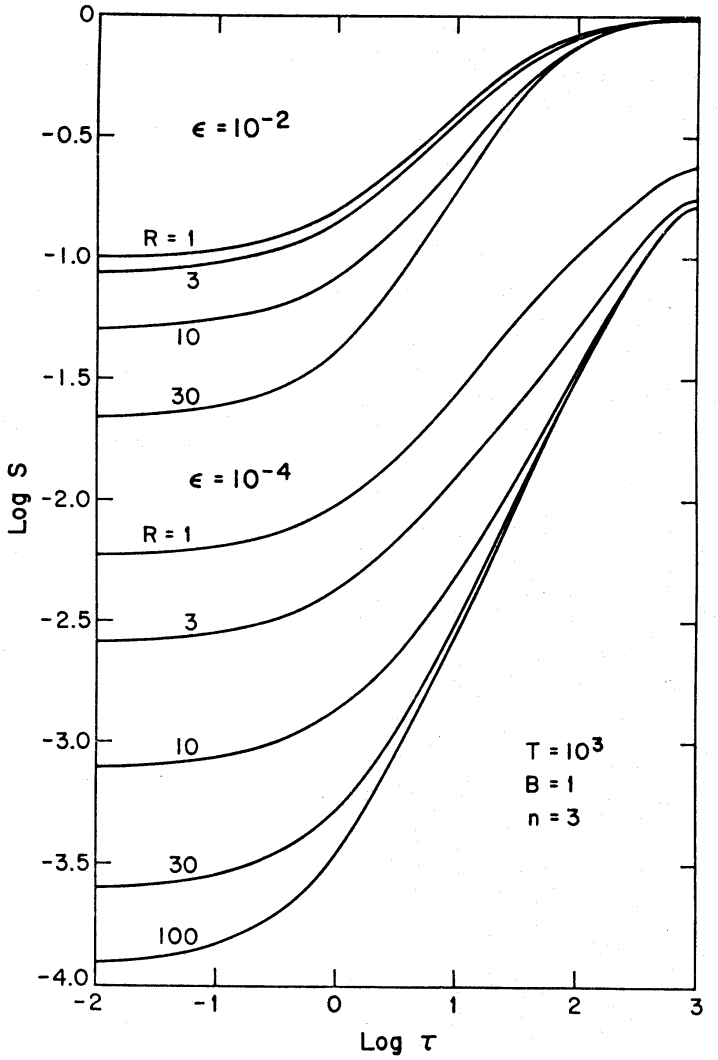

FIG. 5. *Source function vs. optical depth in an atmosphere with* $T = 10^3$, $B = 1$ *and* $k(r) = Kr^{-3}$. *The radius of inner boundary is* $R_c = 1$ *and the radius* R *of outer boundary labels curves.*

In terms of the thermalization length for plane-parallel atmospheres ($\Lambda \sim \epsilon^{-1}$ for Doppler broadening), we see that $S(\tau)$ at $\tau = \Lambda \sim 10^2$ is relatively insensitive to R, i.e. physical conditions here are largely independent of those at the surface. This suggests that the thermalization length for spherical systems will not be very different from that in plane-parallel ones; we speculate that this difference will not exceed the factor $Q(0)$ of Section 3.1 for Doppler broadening or $Q^2(0)$ for Lorentz broadening.

When $\epsilon = 10^{-4}$, $S(\tau)$ lies well below B near the central cavity, since now

$\Lambda \sim 10^4$ and thermalization does not occur. It is interesting that for $R \gtrsim 10$, $S(\tau = T)$ approaches a limiting value of approximately $4{\cdot}46 \times 10^{-2}$. This appears to be the first sign of the large-R limiting form for the source functions in an effectively thin atmosphere. As R increases, $S(\tau)$ assumes this limiting form to larger values of r. This limiting function appears to be roughly proportional to τ throughout most of the atmosphere. The theory of the infinite-R case appears to be both interesting and important.

For $n = 3$ the general behaviour of the source function in Fig. 5 is similar to that for $n = 2$ except that the deviations from the plane-parallel limit are still more extreme. We note that the source functions for $R = 30$, $\epsilon = 10^{-2}$ and $R = 100$, $\epsilon = 10^{-4}$ are similar to those for $n = 2$ with the same values of ϵ and $R = 300$. In the case $n = 3$, $R_t = \sqrt{3}$, $T^{1/2} = 54{\cdot}8$, so that the curve for $R = 100$ is already in the large-R regime. The curves for $R = 10$ and 30 are clearly converging on that for $R = 100$; the spacing of the three curves is quite different from the case of $n = 2$. The limiting curve is again roughly proportional to τ, and the limiting value of $S(\tau = T)$ is 0·166, appearing when $R \gtrsim 3$. It seems that the value of R for which the smaller limit is approached may be explained by examination of the $\tau(r)$ relation (3.61). When $R^{-n+1} \lesssim R_c^{-n+1}$ (= 1 here), it is negligible compared to r^{-n+1} for small r and therefore $\tau(r)$ does not depend on R.

A set of calculations has been made with $\epsilon = 10^{-4}$, $T = 100$, $B = 1$ and $n = 2$, to examine a case in which $R \gg R_t = 100$. The general behaviour of the source functions is similar to that for $\epsilon = 10^{-4}$ shown in Figs. 4 and 5, except that the curves for $R = 30$ and 100 converge nicely to that for $R = 300$; the latter two are essentially identical throughout most of the atmosphere. The comparison with the corresponding results with $T = 1000$ can easily be made from Table VI. Again the limiting curve is proportional roughly to τ. Finally, these results show that $R \gg R_t$ is necessary for $S(0)$ to achieve its limiting value of ϵB.

TABLE VI

Comparison of source functions for $T = 10^2$ and 10^3, $\epsilon = 10^{-4}$, $B = 1$, $n = 2$. In these cases $R_t = 10^2$ and 10^3, respectively.

	$S(\tau = 1)$		$S(\tau = 10)$		$S(\tau = 100)$	
R $T =$	10^2	10^3	10^2	10^3	10^2	10^3
30	3·9−4	1·4−3	1·7−3	4·1−3	1·2−2	2·5−2
100	2·6−4	6·7−4	1·5−3	2·5−3	1·2−2	2·1−3
300	2·2−4	3·9−4	1·5−3	1·8−3	1·2−2	2·0−2

4.2.2 *Models with $B = r^{-2}$.* We turn now to models with $B = r^{-2}$. In Fig. 6 source functions are shown for shells with $T = 10^3$, $\epsilon = 10^{-4}$, $n = 2$ and $R_c = 1$. These results can be compared with the lower set of curves in Fig. 4 (note the difference in the vertical scale!). For the cases shown in Fig. 6, ϵB is much smaller than $S(\tau)$ for all values of τ, while for $B = 1$, $S(0)$ approached ϵB for large R. The most striking feature of the present results is that, when R is large, $S(\tau)$ is roughly proportional to τ^2, in contrast to the τ dependence seen for $B = 1$. Also, we see that $S(0)$ is approximately proportional to R^{-2}, indicating the dominant role of dilution here that was disguised when $B = 1$ by the increase in the photon creation rate towards the surface (for $n = 2$ and 3, with $B = 1$, we found crudely that $S(0) \sim R^{-1/2}$ and R^{-1}, respectively, until the ϵB limit was approached). Because for the cases we consider here the radius changes very little in the region where τ

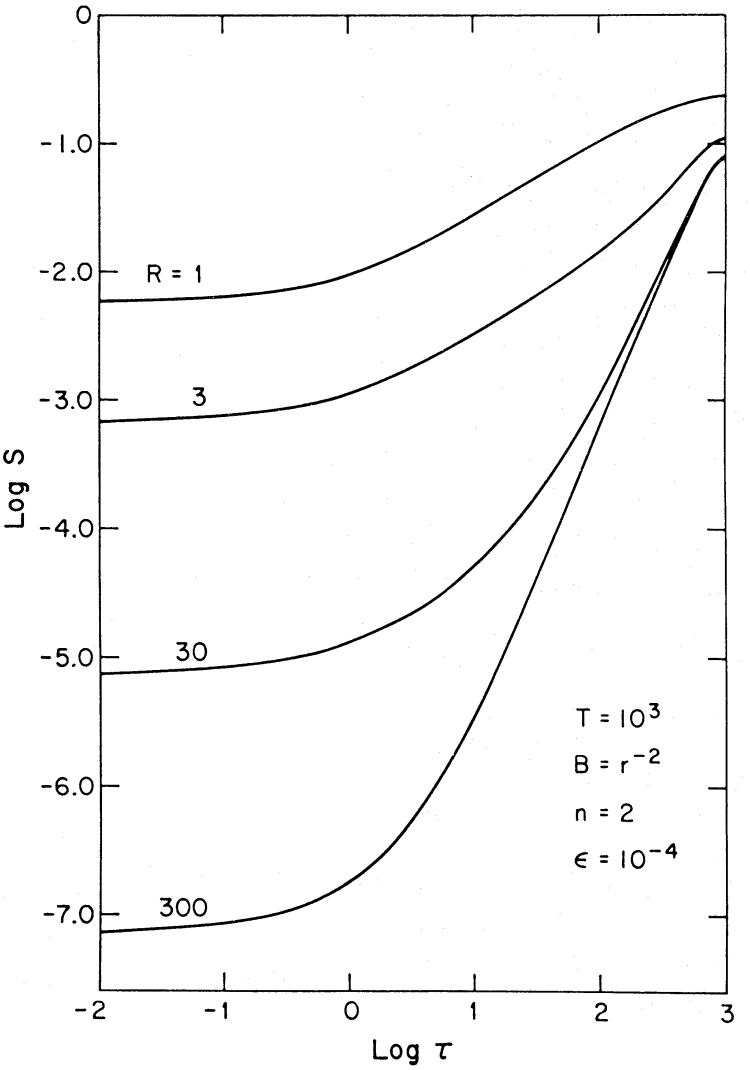

FIG. 6. *Source function vs. optical depth in an atmosphere with* $T = 10^3$, $B = r^{-2}$ *and* $k(r) = Kr^{-2}$. *The radius of inner boundary is* $R_c = 1$ *and the radius* R *of outer boundary labels curves.*

goes from 0 to 1, the source function, which is dominated by diluted radiation flowing up from larger depths in the line wings, is almost constant.

4.2.3 *Mean number of scatterings.* Additional insight into the behaviour of the source functions can be gained from the consideration of the mean number of scatterings defined in Section 3.1.5. In Table VII we give $\langle N \rangle$ as a function of R for shell models with $R_c = 1$, opacity laws $n = 0, 2, 3$, $T = 10^3$ and $\epsilon = 10^{-2}$ and 10^{-4}. In general $\langle N \rangle$ decreases substantially as R increases from R_c, with the initial decrease being quite rapid. For $n = 0$, $\langle N \rangle$ decreases slightly for $\epsilon = 10^{-2}$, and by a factor of roughly 2·4 for $\epsilon = 10^{-4}$, approaching the homogeneous sphere limit in both cases. For $R-3$, $\langle N \rangle$ has dropped to within about 40 per cent and 30 per cent for $\epsilon = 10^{-2}$ and $= 10^{-4}$, respectively, of the large-R values.

For $n = 2$ and 3, with $B = 1$ and $T = 1000$, the decrease in $\langle N \rangle$ as R becomes large is dramatic, particularly for $\epsilon = 10^{-4}$. For $T = 100$, $B = 1$ and $n = 2$, $\langle N \rangle_R / \langle N \rangle_{pl}$ depends on R much as it does for $T = 1000$. However, the results for

TABLE VII

Mean number of scatterings for $T = 10^3$, $R_c = 1$. All results for $B = 1$ except those in parentheses, which refer to $B = r^{-2}$

	$n = 0$		$n = 2$		$n = 3$	
R	$\epsilon = 10^{-2}$	10^{-4}	10^{-2}	10^{-4}	10^{-2}	10^{-4}
1	9·4+1	1·8+3	9·4+1	1·8+3 (1·8+3)	9·4+1	1·8+3 (1·8+3)
3	8·8+1	9·7+2	8·5+1	9·4+2 (1·2+3)	8·4+1	9·5+2 (1·3+3)
10			6·9+1	4·4+2	6·5+1	5·3+2 (1·1+3)
30	8·5+1		4·9+1	2·0+2 (9·1+2)	4·8+1	3·6+2 (1·1+3)
100	8·5+1	7·7+2	2·7+1	7·7+1		2·7+2
300	8·5+1	7·7+2	1·4+1	3·1+1 (8·8+2)		

$B = r^{-2}$ appearing in the table in parentheses, show a much smaller reduction, more like a factor of two. This suggests that, when the rate of photon creation per unit optical depth is constant, escape by one long flight is still the dominant process. The results for $B = 1$ and $n = 2$, 3 are explained largely by the fact that, as R increases, photons are created closer to the outer boundary and therefore escape more readily. Some insight into this effect can be obtained from the mean optical depth for photon creation,

$$\langle\tau\rangle \equiv 4\pi \int_{R_c}^{R} r^2 \epsilon B(r)\, k(r)\, \tau(r)\, dr \Big/ 4\pi \int_{R_c}^{R} r^2 \epsilon B(r)\, k(r)\, dr. \tag{4.2}$$

For $\epsilon B(r) = \text{const.}\ r^{-2}$, we have $\langle\tau\rangle/T = \frac{1}{2}$, independent of $k(r)$, while for $\epsilon B = \text{const.}$, we find that, for $R \gg 1$,

$$\langle\tau\rangle/T \sim \begin{cases} 1/4, & n = 0 \\ \ln R/R, & n = 2 \\ 1/(2 \ln R), & n = 3. \end{cases} \tag{4.3}$$

Thus, since $\langle\tau\rangle$ for $n = 0$ is large and essentially independent of R, we would expect $\langle N\rangle$ to depend only weakly on R and on the form of B. For $n = 2$ and 3, with $B = 1$, $\langle N\rangle$ will decrease rapidly as R increases since $\langle\tau\rangle$ becomes quite small, while with $B = r^{-2}$, $\langle N\rangle$ will be much less sensitive to both n and R, since $\langle\tau\rangle$ is large and constant. The result apparent from Table VII that $\langle N\rangle$ for $\epsilon = 10^{-4}$ and $B = 1$ decreases more rapidly for $n = 2$ than for $n = 3$ is also explained by the behaviour of $\langle\tau\rangle$. It appears that, for a given value of $R \gg 1$, $\langle\tau\rangle$ is smaller for $n = 2$ than for any other value of n.

Very recently Panagia & Ranieri (1973) have published the results of Monte Carlo calculations for constant opacity spherical shells. While they used a Voigt profile with $a = 4{\cdot}72 \times 10^{-4}$, for $T \lesssim 10^3$ the difference from a Doppler profile is negligible and their results are directly comparable with ours. For $B = 1$ their values of $\langle N\rangle$ are in substantial agreement with our $n = 0$ results, to graphical accuracy. However, some of the effects that they seem to imply arise from spherical geometry are in fact found in plane-parallel situations. For $n = 0$ and only moderate values of R/R_c, we would expect only small deviations from plane-parallel behaviour. Much of what they seem to attribute to the effects of spherical geometry in fact arises from the difference between the approximation that photons escape primarily by one long flight and the real transfer process, and has very little to do with geometry.

4.2.4 *Relative importance of single-flight escape, bias in scattering and distribution of photon creation.* For $n = 0$, we have shown that the scattering bias is small and that the distribution of photon creations does not depend sensitively on R. Moreover $S/S_{\rm pl}$ is not significantly different from $1/Q(0)$. In this case it seems that escape according to the longest-single-flight picture is the dominant factor. This is also in accord with the rapid increase of $Q(0)$ as T increases from zero discussed in Section 3.1.4.

For $n = 2$ and $n = 3$, in the case $B = r^{-2}$ for which the photon generation rate per optical depth is constant, the result shown in Table VII that $\langle N \rangle$ is slightly smaller for $n = 2$ than for $n = 3$ is in accord with the slightly larger single-flight escape probability and runs counter to the result expected from the bias argument. The whole question of the importance of the bias clearly needs further investigation, perhaps by Monte Carlo techniques.

4.3 *Emergent radiation*

We now turn our attention to the radiation emerging from spherical atmospheres, confining our attention to calculations with inverse square opacity laws,

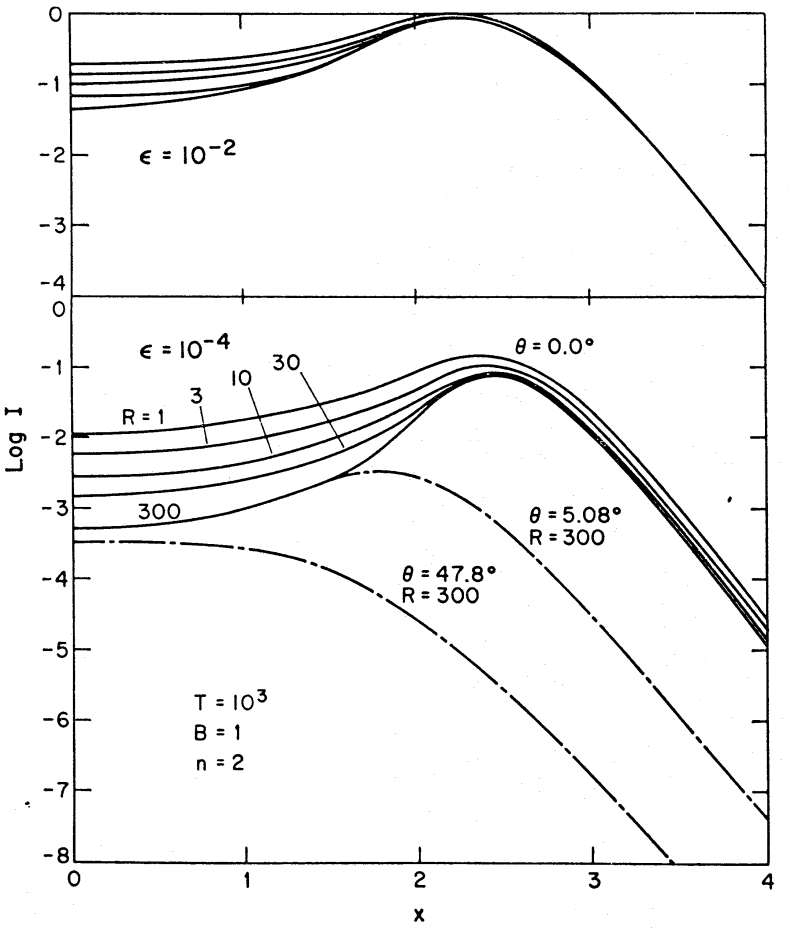

FIG. 7. *Solid lines show frequency dependence of normally emergent intensity from atmospheres with* $T = 10^3$, $B = 1$ *and* $k(r) = Kr^{-2}$, *and are labelled by the radius* R *of outer boundary. Broken curves show, for* $R = 300$, *intensity of radiation emergent at specified angle from normal.* x *is frequency displacement from line centre in units of the Doppler width.*

which suffice to illustrate the general features. In Fig. 7 the normally emergent intensity is shown by solid lines for a series of spherical shells with $T = 10^3$, $B = 1$ and $\epsilon = 10^{-2}$, 10^{-4}, with R going from 1 to 300; the corresponding source functions appear in Fig. 4. In general as θ increases, the characteristic self-reversal rapidly diminishes and finally vanishes. As R increases the angle at which the self-reversal vanishes becomes smaller.

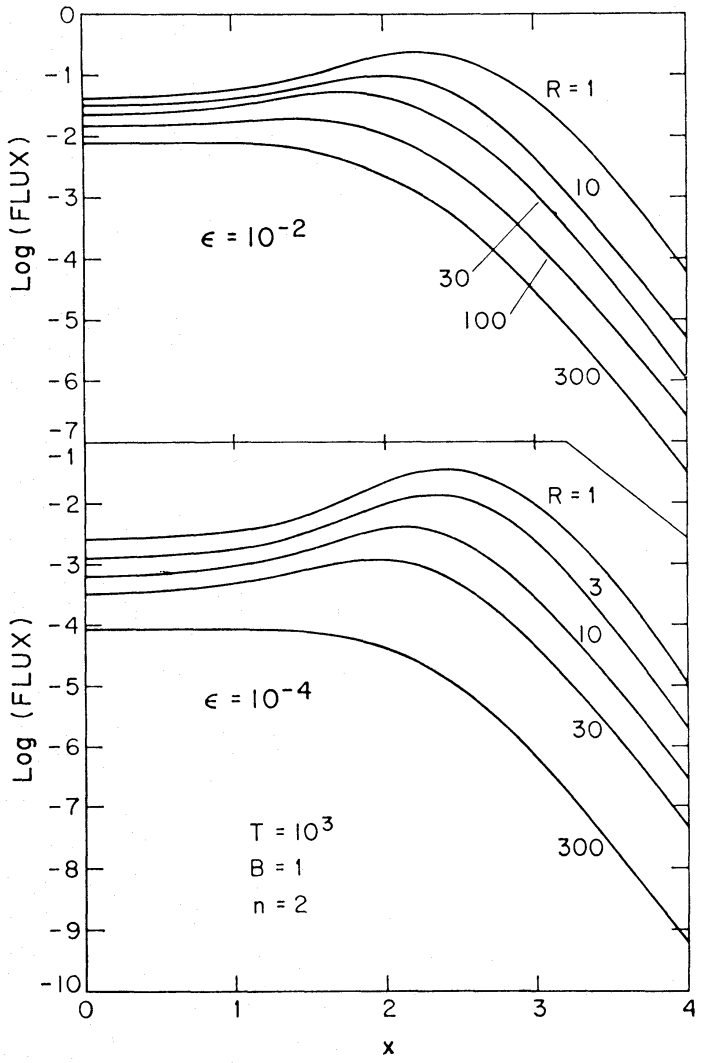

FIG. 8. *Frequency dependence of emergent flux from atmospheres with* $T = 10^3$, $B = 1$ *and* $k(r) = Kr^{-2}$. *Curves are labelled by the radius R of outer boundary.*

One consequence of this very rapid variation of the emergent profile with direction is that, as R becomes large, the self-reversal in the emergent flux diminishes and finally vanishes, as is clear from Fig. 8. When $B = r^{-2}$, the self-reversal is still strong for $R = 300$, but significantly weaker than for the corresponding plane-parallel models.

In Fig. 9, the limb-darkening curves are shown for several frequencies for an extremely extended model with $R = 300$. For comparison the corresponding plane-parallel curves are shown by broken lines for $x = 0$ and 2·4. We note that the limb

darkening is much more severe in the spherical case and depends very strongly on the frequency. In particular, radiation for which $x \gtrsim 2$ is very sharply peaked in the radial direction, as our earlier considerations had suggested. At the largest frequency, $x = 2{\cdot}4$, the atmosphere is optically thin and we see the extreme limit of the forward peaking. The intersection of the short horizontal lines with the curves indicates the angular size of the region, as seen from the outer surface, for which the monochromatic optical depths τ_x exceed unity. This illustrates the angular size of the atmosphere as seen in different parts of the line.

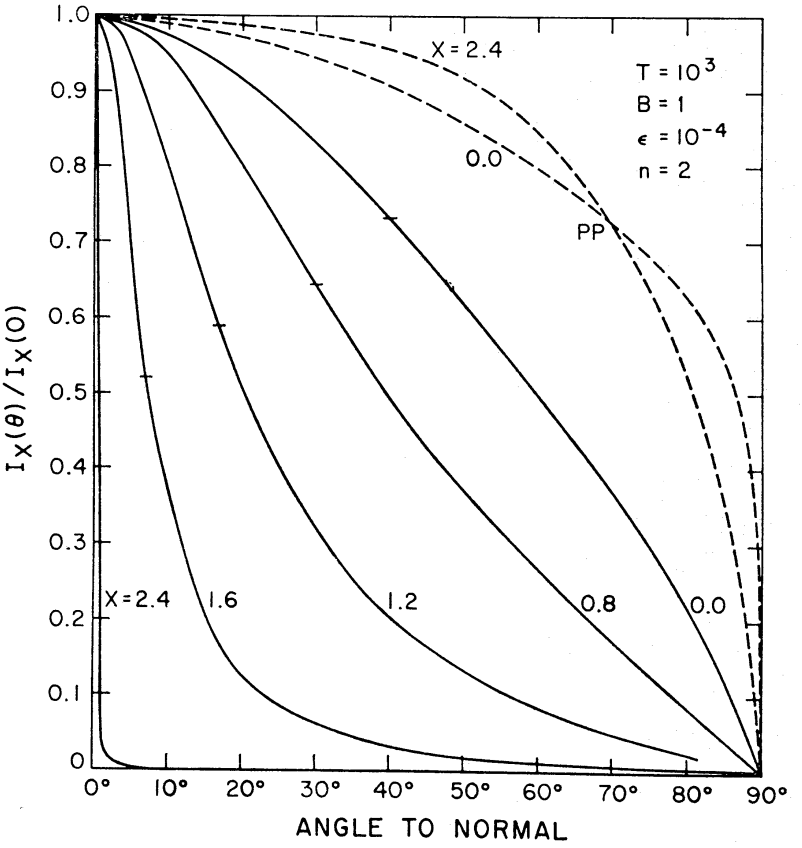

FIG. 9. *Solid curves show angle dependence of limb-darkening for atmosphere with* $R = 300$, $T = 10^3$, $B = 1$, $\epsilon = 10^{-4}$ *and* $k(r) = Kr^{-2}$. *Curves are labelled with frequency variable x. Broken curves are corresponding results for plane-parallel atmospheres.*

4.4 *The internal radiation field*

While the gross features of the internal radiation field have been described in Section 4.2, in the discussion of the source functions, we can examine briefly some of the details from the information in Figs 10 and 11. Both of these figures pertain to models with $T = 10^3$, $\epsilon = 10^{-4}$ and $B = 1$, for which the source function appears in Fig. 4.

In the central parts of the line, where the monochromatic optical depth exceeds unity, the monochromatic mean intensity $J_x(r)$ is seen in Fig. 10 to become nearly independent of frequency, as in the plane-parallel case. As J_x near line-centre is nowhere proportional to r^{-2}, dilution is not the dominant factor, while in the

extreme wings J_x is roughly proportional to r^{-2}. For large values of R we see that J_x, like the emergent flux, does not show the characteristic self-reversal.

The Eddington factors f_x shown in Fig. 11 as functions of the monochromatic optical depth, represent succinctly the angular dependence of the radiation field. The maximum deviations from isotropy are largest in the wing frequencies, where $\mathscr{E}_x$, defined in Section 3.3, is largest, and decreases near the line centre. These deviations also increase significantly with R. For $x \lesssim 2{\cdot}4$, the atmosphere is optically thick and, as expected, f_x approaches 1/3 at large depths. For $x = 3{\cdot}2$, the atmosphere is thin, $\mathscr{E}_x$ is large and throughout most of the atmosphere the radiation

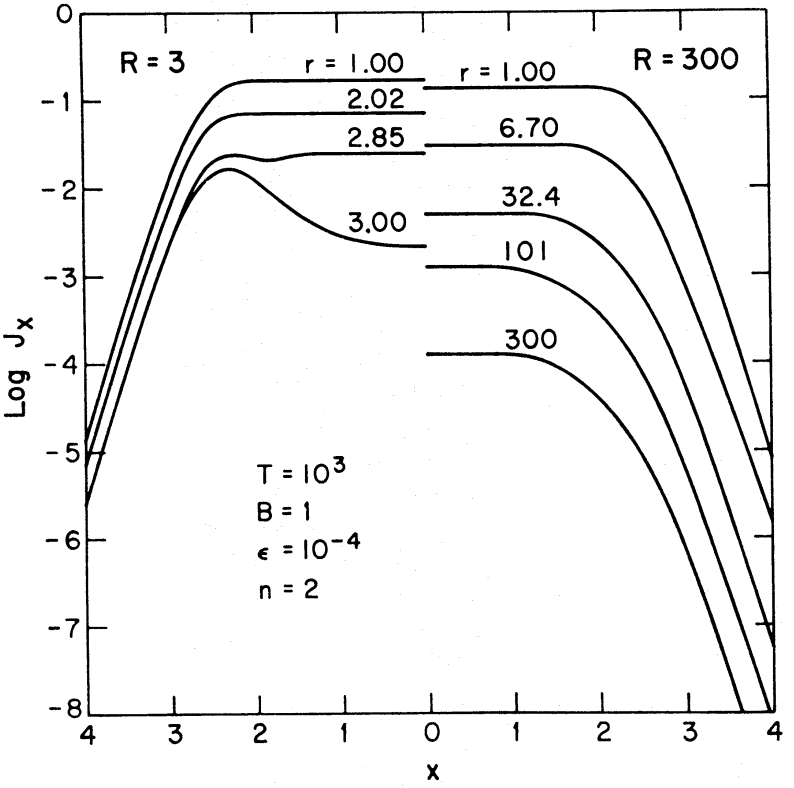

FIG. 10. *Frequency dependence of mean intensity at indicated radii for two atmospheres with* $T = 10^3$, $B = 1$, $\epsilon = 10^{-4}$ *and* $k(r) = Kr^{-2}$. *All curves are symmetrical about* $x = 0$; *curves on left refer to* $R = 3$ *and those on right, to* $R = 300$.

in these frequencies is streaming radially. However, near the central cavity the optical depth perpendicular to a radius vector exceeds that to the surface along the radius vector, with the consequence that the intensity distribution is actually stronger in the perpendicular directions than in the inward radial direction and f_x falls below 1/3. When R is not too large, a similar effect is seen in the core of the line around $\tau = 1$, which occurs near the surface. This effect, which occurs most in plane-parallel situations, does not seem to have been previously recognized.

Although the radiation field in regions of the atmosphere that are optically thin $[\tau\phi(x) \ll 1]$ shows extremely rapid variations with direction and frequency, the results of this section show that the radiation field near line centre, or, more generally, where $\tau\phi(x) \gg 1$, does not behave in a way qualitatively different from that in a plane-parallel situation. Since the source function is dominated by this part of the radiation field, we would expect that the error in assuming complete

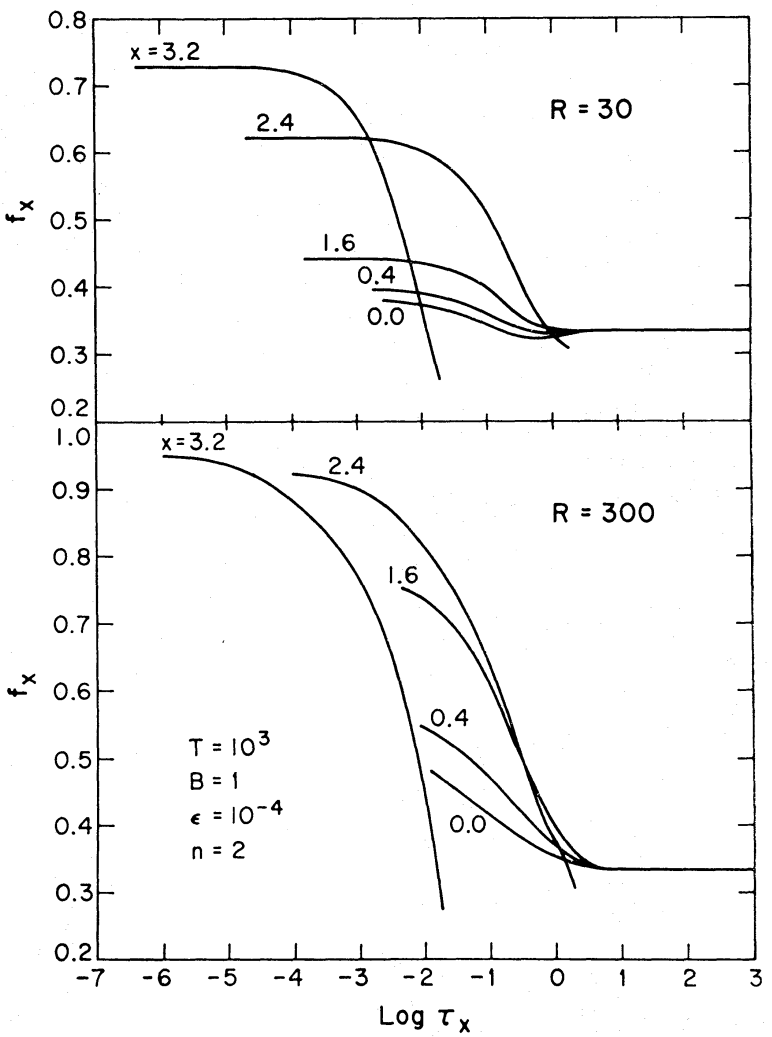

FIG. 11. *Eddington factor* $f_x = K_x/J_x$ *vs. monochromatic optical depth* τ_x *for indicated values of* x, *in atmospheres with* $T = 10^3$, $B = 1$, $\epsilon = 10^4$, $k(r) = Kr^{-2}$, *with* $R = 30$ *and* $R = 300$.

redistribution is not substantially larger for spherical than for plane-parallel atmospheres.

ACKNOWLEDGMENTS

We are very grateful to Dr J. I. Castor and Dr G. B. Rybicki for their aid in understanding the transfer process in spherical atmospheres. Their principal contributions are acknowledged throughout the text. We also wish to thank Chela V. Kunasz for extensive aid with the numerical work, especially for computing the data given in Tables I and II. Finally, we acknowledge with pleasure the support of the National Science Foundation through Grant No. GP-36111.

Joint Institute for Laboratory Astrophysics, University of Colorado, Boulder, Colorado 80302

D. G. Hummer:

Staff member, *National Bureau of Standards and Department of Physics and Astrophysics, University of Colorado*

* Received in original form 1973 June 21

REFERENCES

Aamodt, R. E., 1962. Thesis, University of Michigan.
Abramowitz, M. & Stegun, I. A., 1964. *Handbook of mathematical functions*, p. 244, National Bureau of Standards, AMS55, Washington, D.C.
Ahlberg, J. H., Nilson, E. H. & Walsh, J. L., 1967. *The theory of splines and their applications*, Academic Press, New York.
Auer, L. H., 1971. *J. quantit. Spectrosc. radiat. Transfer*, **11**, 573.
Avrett, E. H. & Hummer, D. G., 1965. *Mon. Not. R. astr. Soc.*, **130**, 295.
Avrett, E. H. & Loeser, R., 1966. *Kernel representations in the solution of line transfer problems*, Smithsonian Astrophysical Observatory Special Report No. 201.
Capriotti, E. R., 1965. *Astrophys. J.*, **142**, 1101.
Cassinelli, J. P. & Hummer, D. G., 1971. *Mon. Not. R. astr. Soc.*, **153**, 9.
Cuperman, S., Englemann, F. & Oxenius, J., 1963. *Phys. Fluids*, **6**, 108.
Cuperman, S., Englemann, F. & Oxenius, J., 1964. *Phys. Fluids*, **7**, 428.
Davison, B., 1958. *Neutron transport theory*, p. 96, Oxford University Press.
Feautrier, P., 1964. *C.r. hebd. Seanc. Acad. Sci. Paris*, **258**, 3189.
Grant, I. P. & Peraiah, A., 1972. *Mon. Not. R. astr. Soc.*, **160**, 239.
Hummer, D. G., Kunasz, C. V. & Kunasz, P. B., 1973. *Computer Physics Communications*, **6**, 38.
Hummer, D. G. & Rybicki, G. B., 1971a. *Mon. Not. R. astr. Soc.*, **152**, 1.
Hummer, D. G. & Rybicki, G. B., 1971b. *A. Rev. Astr. Astrophys.*, **9**, 237.
Ivanov, V. V., 1969. *Stars, nebulae, galaxies*, eds A. A. Boyarchuk, V. V. Ivanov, L. V. Mirzolian, V. V. Sobolev and G. M. Tovmasian, p. 27, Armenian S.S.R. Acad. Sci. Publ. House, Erevan (in Russian).
Ivanov, V. V., 1970. *J. quantit. Spectrosc. radiat. Transfer*, **10**, 681 (in Russian).
Ivanov, V. V., 1973. *The transfer of radiation in spectral lines*, trans. D. G. Hummer, Government Printing Office, Washington, D.C., in press.
Ivanov, V. V. & Nagirner, D. I., 1966. *Astrofizika*, **2**, 147 (English translation: *Astrophysics*, **2**, 75).
Mathis, J. S., 1968. *Resonance lines in astrophysics*, eds R. G. Athay, J. S. Mathis and A. Skumanich, NCAR, Boulder, p. 297.
Nagirner, D. I. & Ivanov, V. V., 1966. *Astrofizika*, **2**, 5 (English translation: *Astrophysics*, **2**, 1).
Panagia, N. & Ranieri, M., 1973. *Astr. Astrophys.*, **24**, 219.
Rybicki, G. B. & Hummer, D. G., 1969. *Mon. Not. R. astr. Soc.*, **144**, 313.
Schmid-Burgk, J., 1973. *Astrophys. J.*, **181**, 865.
Zanstra, H., 1949. *Bull. astr. Inst. Netherl.*, **11**, 1.

APPENDIX

Kernel-Approximation Solutions for the Homogeneous Sphere

The kernal approximation, as introduced by Avrett & Hummer (1965), in which the integral equation for the source function can be solved by approximating the kernel function by a sum of exponentials, has been very useful in the study of radiative transfer in plane-parallel geometries. This technique is used here to obtain, in a very simple manner, accurate numerical solutions for the problem of the homogeneous sphere. While this problem is, as we have indicated in the Introduction, a very special one, it is quite useful in checking more general numerical procedures. Moreover, the homogeneous sphere is currently of some interest in modelling transfer processes in interstellar gas clouds. Although we ignore continuous absorption and emission here, these processes can easily be included in the formulation.

The integral equation for the homogeneous sphere is well known; a convenient discussion of this problem may be found in Davison (1958). If t is the mean optical depth measured from the centre of the sphere ($0 \leq t \leq T$), then the source function $S(t)$ can be obtained from the integral equation for

$$\mathscr{S}(t) = tS(t): \tag{A1}$$

$$\mathscr{S}(t) = (1-\epsilon)\int_0^T [K_1(|t-t'|)-K_1(t+t')]\ \mathscr{S}(t')\,dt' + \epsilon B(t)\,t. \tag{A2}$$

The kernel function $K_1(t)$ is the same function as appears in the analogous plane-parallel problems:

$$K_1(t) = \tfrac{1}{2}\int_{-\infty}^{\infty} \phi^2(x)\,E_1[t\phi(x)]\,dx \tag{A3}$$

and $B(t)$ is the Planck function at the line centre for the local value of the temperature of the particles responsible for the excitation of line photons. We assume here that $B = 1$. As Davison points out, by extending the definition of $\mathscr{S}(t)$ to negative values of t by the relation

$$\mathscr{S}(-t) = -\mathscr{S}(t), \tag{A4}$$

the equation for $\mathscr{S}(t)$ can be written as

$$\mathscr{S}(t) = (1-\epsilon)\int_{-T}^{T} K_1(|t-t'|)\ \mathscr{S}(t')\,dt' + \epsilon t. \tag{A5}$$

Although the similarity to the plane-parallel situation can be further increased by introducing the variable $t' = t+T$, $0 \leq t' \leq 2T$, a more symmetrical formulation is obtained by using the present form.

Let us now introduce the approximate kernel

$$K_1(t) = \sum_{i=1}^{N} a_i\,e^{-b_i t}, \tag{A6}$$

where the constants a_i and b_i have been determined (*cf.* Avrett & Loeser 1966) to provide an accurate fit to the K_1-function. They satisfy exactly the normalization condition

$$\sum_{i=1}^{N} a_i/b_i = \tfrac{1}{2}. \tag{A7}$$

Since $\mathscr{S}(t)$ is an odd function, we look for a solution of the form

$$\mathscr{S}(t) = At + \sum_{\alpha=1}^{N} L_\alpha[e^{-k_\alpha(T+t)} - e^{-k_\alpha(T-t)}], \tag{A8}$$

where the constants A, L_α, and k_α are to be determined. By substituting this expression and that for the kernel into (A5), carrying out the resulting integrations and setting to zero the coefficients of t, $e^{\pm k_\alpha t}$ and $e^{\pm b_i t}$, we obtain the following expressions. The characteristic equation, from which the values of k_α are determined, is exactly as in the plane-parallel case:

$$1 = 2(1-\epsilon)\sum_{i=1}^{N} \frac{a_i b_i}{b_i^2 - k_\alpha^2}, \quad \alpha = 1, 2, \ldots, N. \tag{A9}$$

The coefficient A is unity and the coefficients L are to be calculated from the linear system

$$\sum_{\alpha=1} L_\alpha \left[\frac{1}{1-k_\alpha/b_i} - \frac{e^{-2k_\alpha T}}{1+k_\alpha/b_i}\right] = \frac{1}{b_i}(1+b_iT), \quad i = 1, 2, \ldots, N. \tag{A10}$$

As shown, for example, by Avrett & Hummer (1965), the constants k_α must satisfy exactly the relation

$$\prod_{\alpha=1}^{N} k_\alpha^2 = \epsilon \prod_{i=1}^{N} b_i^2, \tag{A11}$$

which provides a useful check on the numerical solution of the characteristic equation. At the centre of the sphere ($t = 0$), we readily find from (A8) that

$$S(0) = 1 - 2\sum_{\alpha=1}^{N} L_\alpha k_\alpha e^{-k_\alpha T}. \tag{A12}$$

For the mean number of scatterings we have

$$\begin{aligned}\langle N\rangle &\equiv \int_0^T t^2 S(t)\,dt \Big/ \int_0^T t^2 \epsilon B\,dt \\ &= \frac{1}{\epsilon}\left\{1 - \frac{3}{T^3}\sum_{\alpha=1}^{N}(L_\alpha/k_\alpha^2)[e^{-2k_\alpha T}(1+k_\alpha T) - (1-k_\alpha T)]\right\}.\end{aligned} \tag{A13}$$

Since $\mathscr{S}(t)$ is odd, a number of cancellation problems arise in the above equations which did not occur in the plane-parallel problem. The most severe of these occurs in the expression for $\langle N\rangle$, when the quantity in the square brackets in (A13) is subject to cancellation of constant, linear and quadratic terms when $k_\alpha T \ll 1$. Cancellation of the constant terms occurs in the coefficient of L_α in (A10) when both k_α/b_i and $2k_\alpha T$ are very small, and in (A8) when $k_\alpha T$ is very small. In all cases the cancellation can be removed easily by straightforward expansion in the small quantities involved. Values of $S(\tau)$, where τ is the optical depth measured from the surface ($\tau = T - t$), and of $\langle N\rangle$ for scattering with Doppler and Lorentz profiles, are given in Tables III and IV.

While in the plane-parallel case, a closed expression for the emergent intensity $I(x, \mu)$ is readily derived, in the present case the integral expression

$$I(x,\mu) = \phi(x)\int_0^{T\mu} d\xi\, S(t = \sqrt{\xi^2 + T^2(1-\mu^2)})[e^{-\phi(x)(T\mu-\xi)} + e^{-\phi(x)(T\mu+\xi)}] \tag{A14}$$

apparently can not be expressed in closed form. A point of interest here is that, in contrast to the plane-parallel situation in which radiation emerging at an angle arc cos μ contains contributions, albeit very small ones, from the source function at all depths, in the present case the source function is sampled only for t in the interval $T > t > T\sqrt{1-\mu^2}$.